A Quadruple-Porosity Model for Consistent Petrophysical Evaluation of Naturally Fractured Vuggy Reservoirs

Mahaman Salifou Issoufou Aboubacar and **Zhongxian Cai,** China University of Geosciences, Wuhan

Summary

Several dual- and triple-porosity models have been proposed for quantifying the porosity exponent (m) in multiporosity reservoirs. Total porosity (ϕ) is usually portioned into the matrix (ϕ_b) and vuggy porosity, which includes separate vugs (SVGs) and connected vugs (CVGs). As a result, in their majority, the existing petrophysical models were developed and applied mostly without any distinction between the various types of CVGs despite their specific pore geometries, which critically determine the properties of the rock/fluid systems. For instance, unlike otherwise CVGs, natural fractures (NFs) and microcracks that have low pore-aspect-ratio values are highly compressible; this can cause their closure and lead to increasing m values.

In this paper, we proposed a quadruple-porosity model that accounts for NFs (ϕ_2 or ϕ_f) and CVGs (ϕ_c), in addition to ϕ_b and SVGs (ϕ_{nc}) separately, as distinct input variables to ensure accurate determination of m in composite reservoirs. The approach was based on the volume-model method and rules of electric-resistance networks in porous media. Computed water-saturation values used to validate the model show significant improvement and close agreement with the laboratory measurements, demonstrating the applicability of the proposed model for accurate prediction of m in naturally fractured vuggy reservoirs.

New correlations that consider the pore-type diversity were generated using a plot of ϕ vs. m, obtained with the proposed quadruple-porosity model. The procedure involved sorting the ϕ/m scattering points using pore-type mixing and relative abundance of specific porosity. It allowed defining consistent ϕ/m relationships, with determination coefficients of 0.7 to 0.9. This suggests that m varies with the pore-structure types; this was further demonstrated with a rock-frame flexibility factor (γ) used as a proxy to cluster the scattering points. The established correlations can alternatively be applied to reasonably predict m using detailed prior knowledge of pore-type description.

Introduction

Carbonate reservoirs are generally heterogeneous and characterized by complex pore structures showing multimodal pore-type distribution. This complex porosity system strongly affects the petrophysical properties and determines the reservoir rock quality (Morgan and Gordon 1970; Tiab and Donaldson 2004; Ali et al. 2020). This implies that detailed knowledge of pore-type distribution for reliable pore-system characterization is critical to ensure accurate prediction of reservoir parameters (Montaron 2009), in particular the m factor that has been suggested to greatly influence the quantification of fluid saturations used for evaluating reservoir formation (Ragland 2002; Rezaee et al. 2007; Li et al. 2013; Soto et al. 2015; Qin et al. 2016).

The porosity exponent, commonly referred to as the cementation factor, can indicate the degree of rock cementation (lithification) related to compaction under variable confining pressure. Petrophysically, it is a formation property that varies with the pore-path geometrical characteristics, such as tortuosity and connectivity, which condition the conduction ability to fluid or electric current of a porous medium (Melani et al. 2015). Therefore, accurate m estimates can be used as a rock-permeability index (Raiga-Clemenceau 1977; Watfa and Nurmi 1987).

Practically, previous studies have suggested that m relates strongly to the rock lithofacies and pore-system characteristics, such as the rock texture and structure, and amount, structure, and type of porosity, in addition to the external conditions of pressure and temperature (Watfa and Nurmi 1987; Al-Ghamdi et al. 2011; Olusola et al. 2013). Traditionally, using the pioneering work of Archie (1942), which demonstrated that m can range from 1.3 to 2.0 for unconsolidated and highly cemented sandstones, respectively, investigations are conducted to derive m from a log-log plot of ϕ vs. F (the formation-resistivity factor). In such an approach, m is defined as the negative slope of the trendline related through a forced (tortuosity $a = 1$; $\phi = 1$; $F = 1$) or free best fitting. However, this technique is unlikely to be successfully applicable to carbonates with compound pore space comprising matrix porosity, fractures, and vugs (Rezaee et al. 2007; Müller-Huber and Schön 2013). Typically, m varies from $\ll 2$ to ≥ 3 for fractured and vuggy reservoirs, respectively (Towle 1962; Ragland 2002; Soto et al. 2015). This variation can correlate to a decrease and increase of the degree of pore connectedness and tortuosity, respectively (Towle 1962; Lucia 1983; Adisoemarta et al. 2000).

To efficiently quantify m and account for the effect of pore structure on its variation, many attempts have been made using empirical (Ragland 2002; Tabibi and Emadi 2003; Hassanzadeh Azar et al. 2008; Müller-Huber and Schön 2013; Li et al. 2013) and theoretical (Fricke 1924; Rasmus 1983; Serra 1989; Aguilera and Aguilera 2004; Berg 2006; Al-Ghamdi et al. 2011; Olusola et al. 2013; Piedrahita and Aguilera 2017) approaches to accurately derive m in heterogeneous carbonate rocks. However, there remain some technical issues that needed to be addressed for improved prediction accuracy. For example, regarding the difference in the pore-shape factors, portioning touching-vug porosity into fractions of NFs and CVGs could improve petrophysical-modeling and flow-simulation results (Iwere et al. 2002; Pérez-Rosales and Luna 2005; Li et al. 2017) In this paper, we first modified the Al-Ghamdi et al. (2011) improved triple-porosity model derived from the Aguilera and Aguilera (2004) triple-porosity model to establish a quadruple-porosity model. The proposed model allows accounting for the influences of NFs and CVGs separately, in addition to that of matrix and SVG porosities, on the m factor in naturally fractured vuggy reservoirs. Its applicability was then discussed; water-saturation values used as validity criteria were computed to illustrate how the m factor relates to the pore-structure types. Second, we developed new correlations that incorporate the pore-system composition and relative abundance of specific porosity for accurate prediction of m. In addition, the rock-frame-flexibility factor (γ) of Sun (2000, 2004) was used to further investigate the variation of m with the pore-structure types. For illustration,

Original SPE manuscript received for review 8 March 2020. Revised manuscript received for review 10 April 2020. Paper (SPE 201248) peer approved 23 April 2020.

an application example was presented using an available data set related to wells in the study oil field: Tahe Oilfield, North Tarim Basin, China.

Field Description and Typical Multiporosity-Reservoir Rocks

Ordinarily, deeply buried rocks have undergone several diagenetic events that can often lead to the complete modification of depositional facies. Resulting reservoir rocks are usually characterized by low porosity values and various pore structures, which create heterogeneous reservoirs with varied petrophysical properties (Lucia 2007; Dou et al. 2011). The reservoir formations for this study are the Ordovician dolomitic limestones in the Tahe Oilfield of North Tarim Basin, China, which are buried at deeper than 5500 m below the surface. The rock-fabric facies are composed of mudstone/dolostone through grainstone/dolograinstone textures deposited on a ramp/weakly rimmed platform under shallow-water conditions (Ning 2017; Meng et al. 2018). **Fig. 1** shows typical photographs and photomicrographs of reservoir-rock samples, which can demonstrate the intricacy of the porosity system related to the diagenesis. As a result, the reservoir space comprises mostly secondary porosity, and much of the primary porosity has been significantly reduced. The selected full-diameter core samples for water-saturation measurements were analyzed at the laboratory of the Northwest Petroleum Geology Center of SINOPEC using a Dean-Stark method applying the oil-water-saturation-measurement procedure *CPI SY/T5336-2006* (2007). The procedure comprises sample weighing, extraction in organic solvent and heating for approximately 48 hours, collection and measure of the evaporated water volume, oil cleaning, drying and reweighing of the sample, and calculation of the oil volume and different fluid saturations (water and oil).

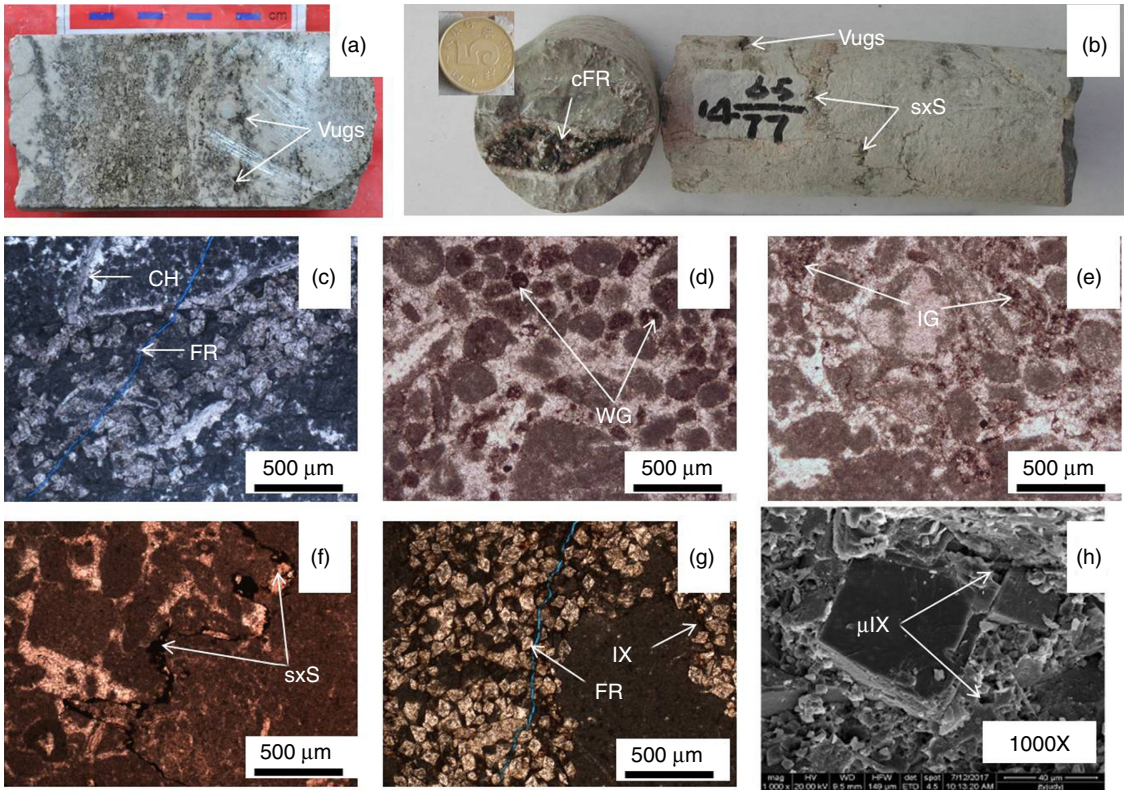

Fig. 1—Typical core thin-section photographs showing multilength-scale reservoir types. (a) A carbonate core of light-gray bioclastic grainstone with oil stains and patches. Note the presence of small-size vugs, interparticle pores, and stylolites. (b) Carbonate (packstone) cores with 10-cm diameter. Note the macroscopic heterogeneity represented by the mixture of intercrystalline space (IX), fracture (FR), dissolved stylolites (S), and vugs, and also calcite cementation within the fractures (cFR). (c) Gray middle crystalline dolomite image with intercrystalline porosity (IX), cemented channel (CH), and fracture (FR). (d, e) Brownish packstone images showing intragranular and intergranular porosity partially filled by bitumen (IG and WG). (f, g) Dolo/packstone-fabric images showing solution-enlarged stylolites partially filled by calcite cement and bitumen (sxS), and intercrystalline porosity (IX) and fracture (FR). (h) Scanning-electron-microscope image at 40-µm scale showing intercrystalline microporosity (µIX).

Previous Works

Admittedly, Archie (1942) pioneered the determination of m using the measured electrical properties (F, R_o) and porosity (ϕ). The method has been widely modified and applied effectively in sandstones that are commonly characterized by uniformly distributed single porosity type (Winsauer et al. 1952; Wyllie and Gregory 1953; Carothers 1968; Porter and Carothers 1970). Although they usually show limited success (Borai 1990), such methods apply also to carbonates, particularly those in which the matrix porosity is prevalent and free of vugs/fractures (Neustaedter 1968; Borai 1987; Hassanzadeh Azar et al. 2008). Typical ϕ/F relationships are interpreter-based, and highly data-driven (site/core-specific) equations that show no clear insight on electrical modeling in porous media, including Archie's equation itself though the physical/theoretical meaning of the parameters (a and m) can be demonstrated (Haro 2006, 2010), and its theoretical basis might exist in the literature (Fricke 1924; Maxwell 1954; Amyx et al. 1960; Pérez-Rosales and Luna 2004, 2005). However, pore-type-mixture and multimodal-porosity systems create strong heterogeneity in the distribution of carbonate physical properties (Lucia 2007), which can prohibit determining m using empirical relationships that likely lead to inaccurate results. Therefore, this poses the need for multiporosity models for accurate determination of m regarding the complexity of the pore systems, and somewhat to the degree of rock-type heterogeneity in carbonate reservoirs.

Different dual-porosity models have been proposed for reservoirs in which the pore space comprises the combination of matrix porosity and vugs, or matrix porosity and fractures. Aguilera (1976) presented a dual-porosity model for estimating the m factor depending on the pore-type mixing and generating charts using the Pickett-like crossplot technique to graphically determine matrix (interparticle) and total porosity in fractured reservoirs. The model was mathematically extended for double-porosity reservoirs with SVGs and/or NFs (Aguilera and Aguilera 2003). The models were dependent on the electric-resistance relationship presented in Pirson (1957). Similarly, several researchers (Serra 1989; Aguilera and Aguilera 2009) conducted dual-porosity modeling using electric-resistance networks for quantifying m in fractured and vuggy reservoirs. In addition, Berg (2006) developed a dual-porosity model using the effective-medium theory. In addition to the fact that the Berg (2006) model considers the porosity exponents of the fracture (m_f) and vugs (m_v), it can also account for m_f values higher than unity, but the determination of m_v is practically problematic (Olusola et al. 2013).

Piedrahita and Aguilera (2017) developed a dual-porosity model to determine m using the parallel-resistance network. The model can specifically enable quantification of fracture-secondary mineralization and tortuosity and estimate their effects on m. Piedrahita and Aguilera (2017) suggested that there is an inverse relationship between m and the mineralization degree and tortuosity of the fracture system. Wang (2017) conceived dual-porosity models using a pore-scale modeling approach to evaluate the effects of vugs (connected and isolated) on electrical properties (F and m) simulated from the finite-difference method. Wang (2017) demonstrated the inconsistency of an in-series resistance-network model in the vuggy reservoirs, and there is a necessity of a decoupling term to account for the effect of CVGs on F and m. Isolated vugs that alter the flow conduction through interparticle porosity affect F and m depending on their shape and size.

Recognizing the obvious porosity-system simplification used for establishing dual-porosity models, triple-porosity models have increasingly become the means to cope with multiporosity reservoirs for consistent petrophysical analysis. This is because different pore classes (intraparticle, moldic/vug, microporosity, interparticle, intercrystalline, and fracture) can actually present specific elastic, petrophysical, and dynamic properties (Gharechelou et al. 2016). Abdassah and Ershaghi (1986) conducted triple-porosity modeling using direct pore simulation (direct numerical simulation) to illustrate the significance of stratal heterogeneity in rock-matrix-layer properties to flow mechanisms in naturally fractured reservoirs. The reservoir space is basically composed of fractures and interparticle pores with different pore sizes. Aguilera and Aguilera (2004) developed a triple-porosity model for petrophysical evaluation of naturally fractured reservoirs. The model that applies to understand the variations in m for a given pore type and its amount was validated through comparison between predicted and measured water saturations. The model was mathematically improved by implementing a rigorous scaling of the different porosities, and the results compare reasonably well with core petrography and numerical data (Al-Ghamdi et al. 2011). The models used a parallel resistance-network for the combination of matrix porosity and fractures (CVGs), and their equivalent medium and SVGs were modeled in series. Olusola et al. (2013) developed dual- and triple-porosity models for quantifying m using electric-resistance networks applying the unified equation of electromagnetic mixing rules (Sihvola 1999). The models were validated theoretically by comparison with previous models (Berg 2006; Aguilera and Aguilera 2009) and practically with core data (Ragland 2002; Byrnes et al. 2006) in the literature.

Approach and Methods

In general, the existing dual- and triple- porosity models that are developed using typical Lucia pore classification group the touching vugs in one single input term (fracture/vug porosity). Lucia (1983, 1995) defined vugs as visible pore space within or significantly larger than the rock particles (i.e., grains and crystals). This includes touching vugs that comprise various space types such as NFs and CVGs (breccias, caves, cavernous, and so forth), which are not necessarily connected to fractures but are directly connected to at least one another to form a long vug/vug-path network, as illustrated in **Fig. 2** (Nair et al. 2008; Sadeghnejad and Gostick 2020). However, although this classification appears genetically/geologically sound, its use can lead to inaccurate results because NFs and CVGs differently affect the rock physical properties because of their peculiarities in the pore morphologies (Saleh and Castagna 2004; Sayers 2008; Xu and Payne 2009). NFs and microcracks that are characterized by low pore-aspect ratio (the short-axis/long-axis ratio) and high sensitivity to stress tend to increase the rock compressibility as a result of their rapid closure under compaction, compared with the ellipsoidal stiff pores such as holes and vugs (Kuster and Toksöz 1974; Mavko and Mukerji 1995; Xu and Payne 2009). Petrophysically, the closure of conductive pores, such as fractures, usually leads to permeability reduction and increase of the formation-resistivity factor (F). Correspondingly, m increases as it relates inversely to the pore-throat radius, both its size and distribution (Wyllie et al. 1958; Jorgensen 1988; Olusola et al. 2013; Müller-Huber and Schön 2013; Wang 2017).

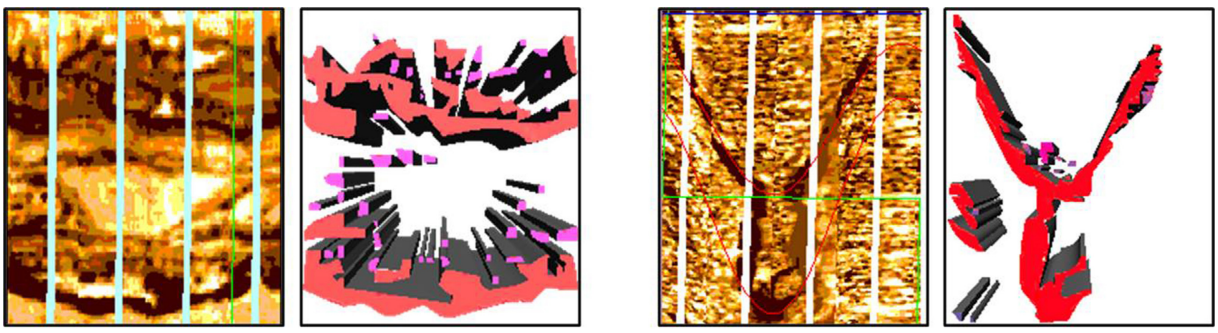

Fig. 2—Typical interconnection between CVGs. (a) Networks of CVGs (red) larger than typical core diameter, and isolated vugs (pink color). Note that coalesced CVGs not attached to the vug networks. Such a vug network can lead to fluid percolation and high horizontal permeability. (b) Dissolution vugs along and attached to the high-angle fracture system (V-shape). Note that vugs are preferentially connected in the vertical direction, which can create high reservoir anisotropy (ratio of the vertical permeability to horizontal permeability).

Practically, numerous studies have demonstrated the sensitivity of physical properties to specific pore morphologies in carbonates. Anselmetti et al. (1998) and Dou et al. (2011) used the perimeter-over-area parameter (γ) and rock-frame flexibility factor (γ), respectively, which both relate strongly to the pore-shape geometry, to show the strong correlation between permeability and pore types. It should be noted that the perimeter-over-area parameter describes the pore roundness and can be defined from the image data,

such as photomicrographs, scanned-electronic microscopic images, and computed-tomography-scanned images. The rock-frame flexibility factor is generally inverted from the velocity, density, and porosity data, and it can be presented as a depth profile attribute. Sayers (2008) used the effective-field theory to quantify the pore-type effect on elastic moduli. Illustrations using actual data showed that low-aspect-ratio pores significantly decrease the elastic moduli for a given porosity. Similarly, Xu and Payne (2009) extended the Xu and White (1996) model by integrating the differential-effective-medium model and Kuster and Toksöz (1974) theory to estimate the pore-type effect on elastic properties. They concluded that ellipsoidal pores (vugs) tend to decrease the rock-acoustic-propagation time, compared with the crack-like pores. On the basis of dual-porosity models, Aguilera and Aguilera (2009) and Aguilera (2010) demonstrated the sensitivity of m to the change in the angle between the fracture dip and the direction of the current flow. This can be particularly relevant for NFs only, though CVGs can be horizontally or vertically interconnected (Fig. 2). Sun et al. (2012) established a differential-effective-medium/Gassmann-equation-based-model to determine the proportions of secondary pores (vugs, holes, and cracks) using the pore-aspect ratio and the Berryman (1995) 3D special pores. Li and Zhang (2018) used 3D rock-physics templates to demonstrate how the sensitivity of elastic properties to the pore-aspect ratio can affect the prediction accuracy of reservoir porosity and saturation. Through simulation of acid-injection performance, Ali et al. (2020) found how the higher acid-propagation velocity relates to NFs compared with vugs, and that the fracture/vug combination would lead to faster and slower propagation at lower and higher injection rates, respectively. In addition to the aforementioned studies, many previous studies illustrated that physical properties relate differently to NFs and CVGs with respect to their pore-shape particularities (eccentricity, pore-aspect ratio), and also their relative abundance (Aguilera and Aguilera 2004). In addition, several workers suggested to portion secondary or vug porosity into fractions of fracture and vug porosities for improved reservoir-simulation efficiency (Iwere et al. 2002; Pérez-Rosales and Luna 2004, 2005). On the basis of these considerations, we determine it to be practical to consider a model that can portion the touching vugs in NFs and CVGs.

Theoretical Modeling. In this study, we established a quadruple-porosity model for estimating m using the volume-model method and electric-resistance networks. The model divides the touching vugs into NFs and CVGs in the sense that m is strongly variable with the pore geometry, and that NFs and CVGs are geometrically different. For this modeling, the term CVG porosity (ϕ_{cv}) was associated here with the CVG. The equation of the quadruple-porosity model, and the Al-Ghamdi et al. (2011) and Aguilera and Aguilera (2004) triple-porosity models are, respectively, given by

$$m=\frac{-\log\left[(\phi_c+\phi_{nc})+\dfrac{(1-\phi_c-\phi_{nc})^2}{\phi_2+(1-\phi_c-\phi_{nc}-\phi_2)/{\phi_b}^{-m_b}}\right]}{\log\phi}, \quad \ldots\ldots (1)$$

$$m=\frac{-\log\left[(\phi_{nc})+\dfrac{(1-\phi_{nc})^2}{\phi_2+(1-\phi_{nc}-\phi_2)/{\phi_b}^{-m_b}}\right]}{\log\phi}, \quad \ldots\ldots (2)$$

$$m=\frac{-\log\left[(\phi_{nc})+\dfrac{(1-\phi_{nc})}{\phi_2+(1-\phi_2)/{\phi_b}^{-m_b}}\right]}{\log\phi}. \quad \ldots\ldots (3)$$

The detailed procedure and schematic used to establish the proposed quadruple-porosity model is presented in Appendix A. The total porosity (ϕ) of the composite system can be given as

$$\phi=\phi_m+\phi_2+\phi_c+\phi_{nc}=\phi_b(1-\phi_2-\phi_c-\phi_{nc})+\phi_2+\phi_c+\phi_{nc}. \quad \ldots\ldots (4)$$

It can be demonstrated that the proposed quadruple-porosity model applies for all combinations of matrix, fracture, CVG, and SVG porosities. For simplicity and clarity, the different models were derived using the porosity system and possible pore-type combinations. For a triple-porosity system, there are four models derived from possible pore-type combinations. The modeling requires two steps for the cases made out of fractures and any couple of two of the three other pore types (ϕ_b, ϕ_c, and ϕ_{nc}), which, if occurring together, can be modeled using a series-resistance network. For a double-porosity system, six models can be derived from possible pore-type combinations. The parallel resistance network is applicable to the cases made out of fractures and each one of the three other pore types, which can be modeled as in a series-resistance network for any combination of two of them. Finally, four models exist for the cases comprising only a single pore type. The theoretical graphical demonstrations for the $(\phi_b+\phi_2+\phi_{nc})$, $(\phi_b+\phi_2)$, $(\phi_b+\phi_{nc})$, and $(\phi_{nc}+\phi_2)$ combinations were given in Aguilera and Aguilera (2004), Al-Ghamdi et al. (2011), and Olusola et al. (2013). The graphical theoretical demonstrations for the $(\phi_b+\phi_2+\phi_c)$, $(\phi_b+\phi_c+\phi_{nc})$, $(\phi_c+\phi_2+\phi_{nc})$, $(\phi_b+\phi_c)$, and $(\phi_c+\phi_2)$ combinations are subject for further works. **Table 1** summarizes the different possible theoretical derivative models for monoporosity, dual-porosity, and triple-porosity systems.

The derivation showed that the assumption in which a reservoir includes SVGs and/or CVGs only led to $m=0$, which, practically, sounds not reasonable. The case of a reservoir including SVGs only has already been presented in the literature (Focke and Munn 1987), and researchers (Aguilera and Aguilera 2003; Olusola et al. 2013) have suggested its abstract nature with respect to the possibility of hydrocarbon migration and drainage into the vugs. This is likely applicable to the cases of reservoirs with CVGs, and SVGs and CVGs only. In addition, it can be explained because CVGs are typically associated with secondary dissolution, which occurs generally along fractures/faults, and through interparticle porosity that could provide the fluid-circulation routes, particularly in grainstones and packstones with relatively high interparticle permeability (Smith et al. 2003; Lønøy 2006).

Model Validation. The first step in the evaluation of the model was to compare the m values calculated with the proposed quadruple-porosity model with those obtained using the Aguilera and Aguilera (2004) triple-porosity model and Al-Ghamdi et al. (2011) improved triple-porosity model. For the two models involved for comparison, we calculated m using two hypotheses in which the term ϕ_2 was assumed to first represent touching vugs (CVGs+NFs), as defined by Lucia (1983), and second to represent equal to NFs only. It should be noted that the first hypothesis represents the ideal conditions of the two triple-porosity models, and the second one implies that the reservoir contains no CVGs. Subsequently, after determining the m values, water saturations were computed and used as validity criteria in the sense that the porosity exponent, m, can account for the major source of uncertainty in the determination of water saturation in a multiporosity reservoir, particularly using the Archie equation (Focke and Munn 1987). The results obtained were compared with laboratory water-saturation measurements from full-diameter core samples.

$$m=\frac{-\log\left[\left(\phi_c+\phi_{nc}\right)+\frac{\left(1-\phi_c-\phi_{nc}\right)^2}{\phi_2+\left(1-\phi_c-\phi_{nc}-\phi_2\right)/\phi_b^{-m_b}}\right]}{\log\phi}$$

$m=\frac{-\log\left[\left(\phi_{nc}\right)+\frac{\left(1-\phi_{nc}\right)^2}{\phi_2+\left(1-\phi_{nc}-\phi_2\right)/\phi_b^{-m_b}}\right]}{\log\phi}$	$m=\frac{-\log\left[\frac{1}{\phi_2+\left(1-\phi_2\right)/\phi_b^{-m_b}}\right]}{\log\phi}$	$m=m_b$
	$m=\frac{-\log\left[\phi_c+\left(1-\phi_c\right)\phi_b^{-m_b}\right]}{\log\phi}$	
$m=\frac{-\log\left[\left(\phi_c\right)\frac{\left(1-\phi_c\right)^2}{\phi_2+\left(1-\phi_c-\phi_2\right)/\phi_b^{-m_b}}\right]}{\log\phi}$		$m=1$
	$m=\frac{-\log\left[\phi_{nc}+\left(1-\phi_{nc}\right)\phi_b^{-m_b}\right]}{\log\phi}$	
	$m=\frac{-\log\left[\phi_c+\frac{\left(1-\phi_c\right)^2}{\phi_2+\left(1-\phi_c-\phi_2\right)}\right]}{\log\phi}$	$m=0$
$m=\frac{-\log\left[\left(\phi_c+\phi_{nc}\right)\frac{\left(1-\phi_c-\phi_{nc}\right)^2}{\phi_2+\left(1-\phi_c-\phi_{nc}-\phi_2\right)}\right]}{\log\phi}$		
	$m=\frac{-\log\left[\left(\phi_{nc}\right)+\frac{\left(1-\phi_{nc}\right)^2}{\phi_2+\left(1-\phi_{nc}-\phi_2\right)}\right]}{\log\phi}$	$m=0$
$m=\frac{-\log\left[\left(\phi_c+\phi_{nc}\right)+\left(1-\phi_c-\phi_{nc}\right)\phi_b^{-m_b}\right]}{\log\phi}$		
	$m=0$	

Table 1—Derived theoretical models using possible combinations of pore types and porosity systems. In the top row is the quadruple-porosity-model equation. (Left to right) The first column (left) shows the triple-porosity models related to (ϕ_b+ϕ_{nc}+ϕ_2), (ϕ_b+ϕ_c+ϕ_2), (ϕ_c+ϕ_{nc}+ϕ_2), and (ϕ_b+ϕ_c+ϕ_{nc}) pore combinations from top to bottom, respectively. The second column (center) includes the dual-porosity models for the (ϕ_b+ϕ_2), (ϕ_b+ϕ_c), (ϕ_b+ϕ_{nc}), (ϕ_c+ϕ_2), (ϕ_{nc}+ϕ_2), and (ϕ_c+ϕ_{nc}) combinations from top to bottom, respectively. The third column (right) are the models for a single-porosity system made of only matrix (ϕ_b), NFs (ϕ_2), CVGs (ϕ_c), and SVGs (ϕ_{nc}), from top to bottom, respectively. The total porosity ϕ can be substituted for any combination.

The total porosity was determined and portioned into fractions of its components using the approach and modeling procedure presented in Issoufou Aboubacar et al. (*In press*). Briefly, the procedure of the total porosity determination and partition applies the rock-physics models and rock-digital-image-analysis techniques. The laboratory measurements are conducted at the full-diameter-core and core-plug scales to determine the total and matrix porosity, respectively. In addition, digitized core images, computed-tomography-scanned images, thin-section-derived photomicrographs, and borehole electrical images are processed to quantify porosities at different scales using a pixel-counting technique, and the standard radioactive and acoustic-porosity logs are inverted to derive the total and matrix/interparticle porosity, respectively. For comparable cored intervals, calibration and comparison between the different porosities enable us to generate correlations, which are successfully applied to establish the porosity profiles for the full reservoir depth.

Developing New Correlations for Porosity-Exponent Prediction. Correlations are widely applied in practice to derive m in well-logging interpretation, mostly in the absence of sufficient laboratory measurements. However, regardless of the site-specific or highly data-driven nature, accurate correlations should consider the influence of the rock lithology (Focke and Munn 1987; Müller-Huber and Schön 2013), and the change in pore-structure types most importantly (Myers 1991; Wang and Lucia 1993; Ragland 2002). Therefore, this study presents a new correlation procedure that accounts for the pore-type composition and distribution through the sorting of scattering points. This involved plotting ϕ and m along the x- and y-axis, respectively; m was obtained with the proposed quadruple-porosity model. In addition, we attempted to quantify the pore-type effects on the variation of m by using a rock-frame-flexibility factor (γ). The procedure used to determine the γ factor was similar to that in Sun (2000, 2004) and in Appendix A appearing in Dou et al. (2011). The γ factor is a geometrical parameter that strongly depends on the connectivity of the solid matrix/pore system and rock texture, but importantly on the pore structure in carbonate reservoirs. It can be calculated using the density, porosity, and sonic log data; it can also be estimated from the core and seismic data (Sun 2000).

Results and Interpretation

Determination of m and S_w. In this subsection, the applicability of the proposed quadruple-porosity model to accurately determine m in multiporosity systems was investigated using common core and well-log measurements. As described in the preceding Model Validation subsection, m was calculated with the model proposed in this study, the Aguilera and Aguilera (2004) triple-porosity model, and the Al-Ghamdi et al. (2011) improved triple-porosity model, with the two hypotheses in mind. **Fig. 3** shows the m/depth profiles related to the different formulations. Except for the first hypothesis with the triple-porosity model (m_1) and its improved version (m_3) at some horizons, the m values obtained are in general high. Typical values are proper to low-porosity (<5%) tight reservoirs (Hassanzadeh Azar et al. 2008), and vuggy reservoirs (Focke and Munn 1987). However, it can be observed that each m/depth profile exhibits large variations, which likely correlate with the pore-structure changes along the reservoir depth. It can also be seen that the different m profiles overlap opposite horizons without CVGs, demonstrating the match between the different formulations. In contrast, opposite the horizons with CVGs, there is a departure between the m/depth profile related to the proposed quadruple-porosity model (m_5) and those from the triple-porosity model, m_1 and m_2 (Aguilera and Aguilera 2004) and improved triple-porosity model, m_3 and m_4 (Al-Ghamdi et al. 2011), which show nearly identical trends for a given hypothesis. Importantly, the difference increases with increasing CVGs

(ϕ_c), and it becomes more significant in horizons with relatively low matrix and fracture porosities. The largest separation is observed between the m_5-depth profile and the m_1 and m_3 related profiles for the first hypothesis (ϕ_2 = CVGs+NFs), which meets the formatting in the two triple-porosity models. On the other hand, for the second hypothesis, the m_5 values do not significantly depart from the m_2 and m_4 values obtained with the triple-porosity model and its improved version, respectively. In addition, the results clearly show that something must be wrong because physically, m should be nearly equal to 2 (m_b) and greater than in horizons significantly dominated by matrix porosity and SVGs, respectively. For example, some horizons in which SVGs comprise higher than 50% of total normalized porosity show $m < 2$ (1.2 to 1.7), such as 5737 to 5745 m, 5757 to 5758 m, and 5768 to 5775 m (Fig. 3, Tracks 4 and 6). But, it should be noticed that these horizons are characterized in general by a nonnegligible proportion of CVGs (5 to 20% total normalized porosity), indicating how CVGs can significantly influence m (Berg 2006). Overall, the results obtained with the triple-porosity models appear unusual and probably not reasonable. However, because the measured m values are not available, it is not possible to statistically determine the prediction accuracy of the proposed model using the m factor directly.

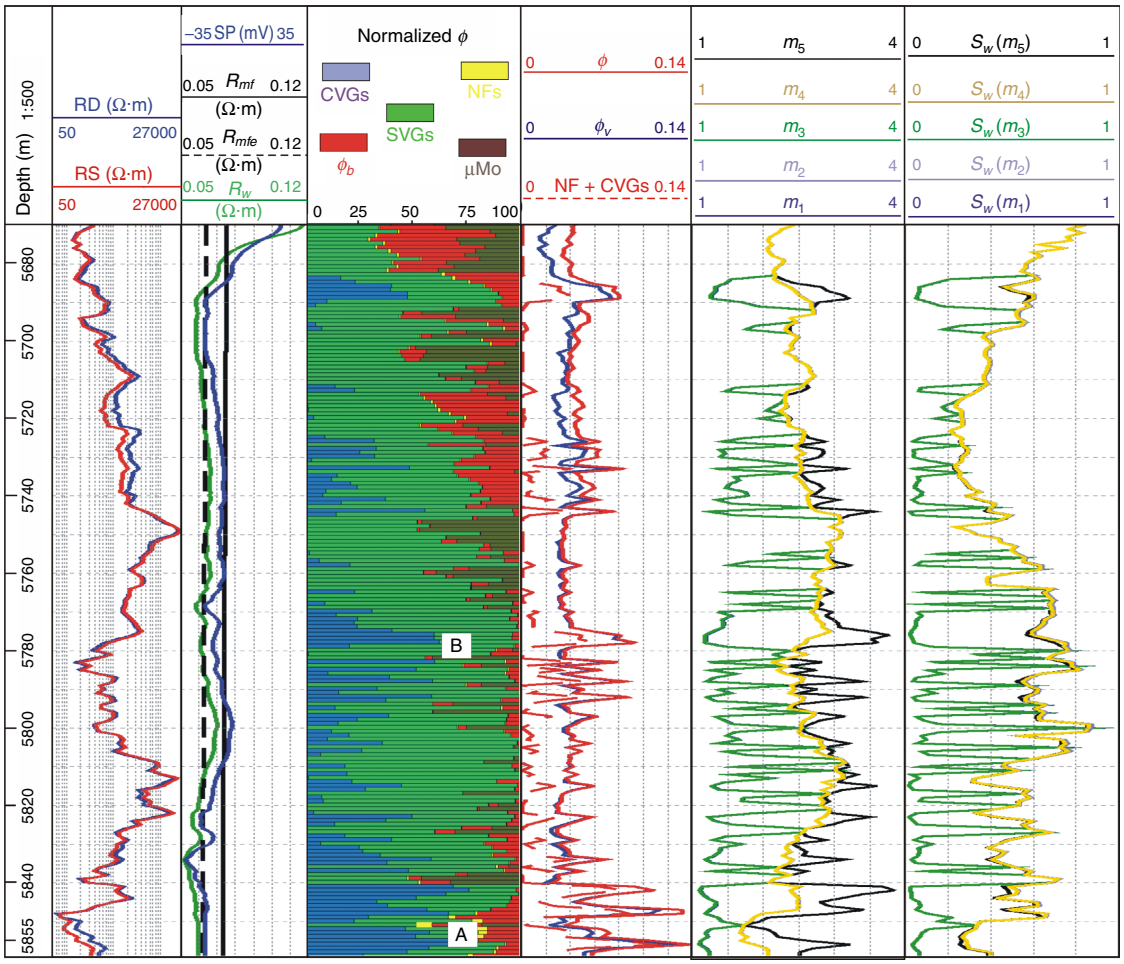

Fig. 3—Computation comparison of the depth profiles of the porosity exponent and water saturation. (Left to right) Track 1 is the depth (in m). Track 2 is the deep-resistivity (RD) (in Ω·m) log and shallow-resistivity (RS) (in Ω·m) log. Track 3 is the spontaneous potential (SP), R_m, R_{mf}, and R_{mfe} logs. Track 4 is the porosity-partition map showing how the pore-type composition can change along the reservoir depth. The porosities are given in the percentage of total normalized porosity, and points *A* and *B* are used to illustrate the variations of the porosity exponent (m) with the pore-type composition rather than the total porosity (Fig. 5a). Track 5 is the curves of total porosity (ϕ), total vuggy porosity (ϕ_v), and touching-vug porosity (NFs+CVGs). Track 6 is the m/depth profiles, m_1 = triple-porosity model [ϕ_2 = NFs+CVGs; Aguilera and Aguilera (2004)]; m_2 = triple-porosity model [ϕ_2 = NFs; Aguilera and Aguilera (2004)]; m_3 = improved triple-porosity model [ϕ_2 = NFs+CVGs; Al-Ghamdi et al. (2011)]; m_4 = improved triple-porosity model [ϕ_2 = NFs; Al-Ghamdi et al. (2011)]; m_5 = proposed quadruple-porosity model (this study). Track 7 is the S_w/depth profiles established using the m/depth profiles shown here in Track 6. The S_w/depth profiles are numbered consistently with the m/depth profiles.

Therefore, the relevance of determining accurate m values for petrophysical evaluation was demonstrated according to water-saturation estimation because its accuracy largely depends on the reliability of m, among others (Fig. 3, Track 6). In doing so, water saturations used for model validation were computed with m values obtained with the different formulations. Assuming that the determined m values are accurate, in addition, the studied formations are relatively clean, with low-enough shale volume (<4%) that might not significantly affect the petrophysical parameters (Hilchie 1978); water saturation was therefore calculated using the Archie equation (Al-Ghamdi et al. 2011). Importantly, this can allow the back calculation of electrical parameters (F and R_o) after identifying 100%-water-saturated horizons. The tortuosity factor (a) and saturation exponent (n) were taken as constant and equal to 1 and 2, respectively, although they should be obtained using core analysis and are not necessarily constant (Myers 1991; Mahood and Boyd 1993; Adisoemarta et al. 2000; Ramamoorthy et al. 2019). The formation-water resistivity (R_w) was determined from the actual drilling-mud properties. This can ensure accurate determination of R_w, although it should be directly measured in the laboratory. The applied procedure is given in Appendix B. **Table 2** shows the main input data, computed and measured values for five cored intervals.

Depth (m)	ϕ_c	ϕ	ϕ_v	ϕ_{nc}	ϕ_f	ϕ_b	ϕ_m	ϕ_{f+c}	R_w	R_t	m_1	S_w (m_1)	m_3	S_w (m_3)	m_2	S_w (m_2)	m_4	S_w (m_4)	m_5	S_w (m_5)	S_w (Core)
5692–5703 (1)	0.001	0.047	0.039	0.039	0.000	0.007	0.007	0.001	0.059	589.009	2.365	0.410	2.354	0.403	2.450	0.458	2.439	0.450	2.447	0.449	0.50
5712–5722 (2)	0.002	0.046	0.031	0.029	0.000	0.014	0.014	0.002	0.063	1273.37	2.100	0.202	2.092	0.200	2.342	0.279	2.336	0.276	2.370	0.276	0.30
5736–5750 (3)	0.008	0.047	0.042	0.034	0.000	0.005	0.005	0.008	0.065	7738.82	2.127	0.173	2.116	0.170	2.807	0.355	2.958	0.350	2.952	0.348	0.35
5781–5801 (4)	0.015	0.050	0.047	0.032	0.000	0.003	0.003	0.015	0.066	647.092	1.736	0.282	1.725	0.277	2.464	0.684	2.255	0.673	2.715	0.663	0.55
5846–5848 (5)	0.050	0.094	0.078	0.027	0.001	0.015	0.014	0.063	0.058	264.992	1.260	0.074	1.246	0.073	3.160	0.594	3.150	0.587	3.096	0.555	0.55

Table 2—Comparison of the results from the example application. m_1 = triple-porosity model [ϕ_2 = NFs+CVGs; Aguilera and Aguilera (2004)]; m_2 = triple-porosity model [ϕ_2 = NFs; Aguilera and Aguilera (2004)]; m_3 = improved triple-porosity model [ϕ_2 = NFs+CVGs; Al-Ghamdi et al. (2011)]; m_4 = improved triple-porosity model [ϕ_2 = NFs; Al-Ghamdi et al. (2011)]; m_5 = this study. S_w (m_1) through S_w (m_5) are the water-saturation estimates based on m_1 through m_5, respectively. Constants applied for S_w calculation are $a = 1$, $m_b = 2$, $m_f = 1$, and $n = 2$. The procedure applied for R_w determination is given in Appendix B. Total porosity $\phi_v = \phi_c + \phi_{nc}$.

Establishing Consistent Correlations for Porosity-Exponent Prediction. **Fig. 4** is a crossplot of ϕ vs. m, obtained with the proposed quadruple-porosity model. The plot shows a substantial scattering that becomes more significant at higher porosity, indicating no clear m/ϕ relationship in these reservoirs. In addition, it can be seen that m varies regardless of the porosity range, showing also that no consistent correlation can be established as a function of porosity range, both for the low-porosity ($\phi < 5\%$) and high-porosity ($\phi > 5\%$) zones (Fig. 4a). However, it can be seen that the porosity exponent m exhibits an apparent tendency to increase as ϕ increases. This observation is consistent with the literature [i.e., the higher m values relate to high porosity, although m varies with the pore-type composition rather than the total porosity (Focke and Munn 1987; Byrnes et al. 2006)].

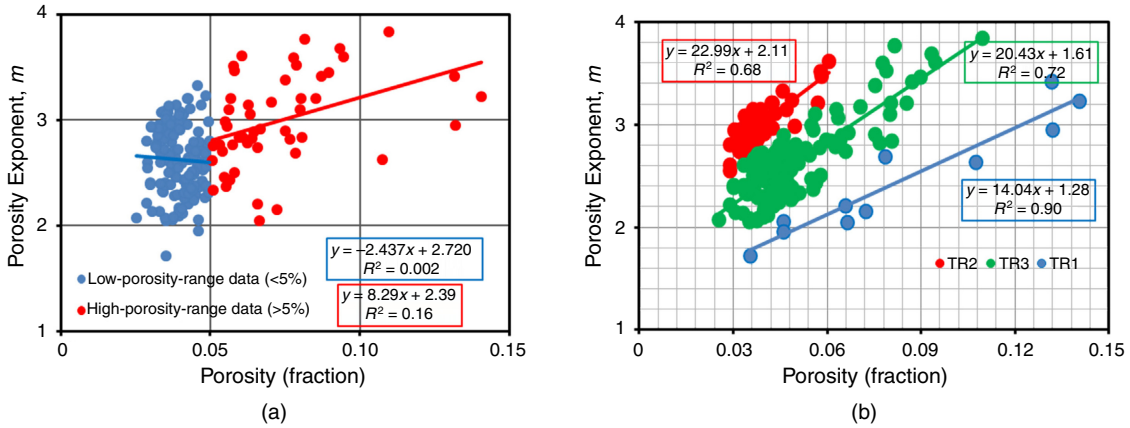

Fig. 4—Plot of porosity vs. porosity exponent. (a) Variation of *m* with total porosity and porosity range; the results show no direct correlation. (b) Data in (a) grouped according to pore-type mixing and porosity abundance. This results in highly acceptable correlations, indicated by the coefficients of determination from 0.7 to 0.9. TR1 is related to the points colored in blue, and CVGs dominate the pore-type composition. TR2 is for points colored in red, with SVGs as the prevalent pore type. TR3 is associated with the points colored in green, and the pore type is generally a mixture of SVGs and matrix porosity.

To test the assumption of the strong influence of pore-structure changes on reservoir petrophysical properties (in particular, m in this study), we grouped the scattering points according to pore-type mixing and relative abundance of specific porosity. This has enabled us to generate consistent trends between ϕ and m, which could be applied to predict reasonable m values using detailed knowledge of pore-system composition and distribution (Fig. 4b). R^2 (determination coefficients) varies from 0.7 to 0.9. A reliable porosity-system description can be achieved, both qualitatively and quantitatively, from core and/or thin-section data (Lønøy 2006; Bahrami et al. 2017). The results demonstrate well that m correlates strongly with the porosity system and the abundance of specific porosity in such carbonate reservoirs, rather than the scalar total porosity (Towle 1962; Ehrlich et al. 1991). It can also be seen that m exhibits a tendency to increase with the abundance of near-spherical pores. This is consistent with the observation of Towle (1962) and Focke and Munn (1987). In Fig. 4b, coherent trend lines as shown were defined, clearly relating m to the porosity system or pore-type mixing. The used color codes are consistent for the scattering points, fitted trendlines, and related equation labels. The blue-color features represent the vuggy porosity systems dominated significantly by CVGs (approximately 65%), with fracture porosity reaching nearly 2.5%. The porosity value averages 8.4 in the porosity unit. This was referred to as the first trend/relational equation (TR1). The red-color features are associated with the vuggy porosity systems in which SVGs are largely dominant (86%), but matrix porosity can reach up to 40% in some horizons [referred to as the second trend/relational equation (TR2)]. In particular, the large part of the SVGs is micromoldic porosity (μMo). The porosity value is in general low, >3.5 p.u. The green-color features correspond to mixed-porosity systems dominated significantly by the combination of SVGs (approximately 60%) and matrix porosity (25%). But there is no dominant pore type in some horizons [referred to as the third trend/relational equation (TR3)]. Note that the porosity values are reported in the percentage of total normalized porosity, if not indicated.

Furthermore, we colored the scattering points with the frame-flexibility factor (γ) to further test the theory of the significant influence of pore-structure types on physical properties (velocity, permeability, and m) in carbonates (Sun 2000, 2004). The points with $\gamma \leq 2.4$ and >6.5 are colored in blue and red, respectively, and the other points with γ between 2.4 and 6.5 are shown in green **(Fig. 5a).** Despite the substantial overlap between the points colored with the intermediate and high values of γ, particularly for the low-porosity values, the scattering points show distinct clusters, and both ϕ and m vary inversely with γ. The overlap could result because of the difficulties to distinguish the microintercrystalline porosity from moldic separate-vug porosity, Mo (Huang et al. 2017). Again, the results showed that m varies with the pore-type composition most importantly, rather than the numerical total porosity value. This suggests that

establishing reliable correlations for predicting m should take into account the pore-structure heterogeneity. For example, the points A and B have nearly the same bulk porosity ϕ of approximately 7.9%, but their m values are 2.69 and 3.52, respectively, a difference of nearly unity (approximately 0.83) (Fig. 5a). This resulted because point A has a relatively high fraction of matrix and fracture porosity (approximately 10% of total normalized porosity), compared with point B, with lower abundance of interparticle and fracture porosity (approximately 4% of total normalized porosity), but the significant portion of their total porosity comprises vuggy porosity (SVGs and CVGs). From the poroelasticity perspective, whereas low γ values relate to high-velocity medium and/or porosity systems essentially composed of visible vuggy and/or intercrystalline porosity at a given porosity, high γ values indicate low-velocity medium and/or porosity systems dominated by interparticle and crack-like pore space (Sun 2000, 2004; Dou et al. 2011). This can be verified with the present illustration (Figs. 3 and 5b). For the points with high γ values ($\gamma > 6.5$) shown in red, the total porosity is dominated by the mixture of matrix and SVGs; both fracture porosity and micromoldic SVG porosity (μMo) occur in a relatively appreciable percentage, while the CVG is very limited. For the points colored in green ($2.4 < \gamma \leq 6.5$), their total porosities comprise a mixture of all different occurring pore types. But, the SVGs/CVGs are prevalent, and μMo is relatively more abundant compared with ϕ_f. The total porosity is volumetrically composed of CVGs (>55% of total normalized porosity) for points colored in blue ($\gamma \leq 2.4$). It should be noted that the selection of the γ cutoff values is interpreter-based, and they are set in such a way to distinguish the different groups of points. The values can vary for different reservoirs according to the value range, and calibration of γ values to core data is required for pore-type classification on the ϕ/m crossplot (Dou et al. 2011).

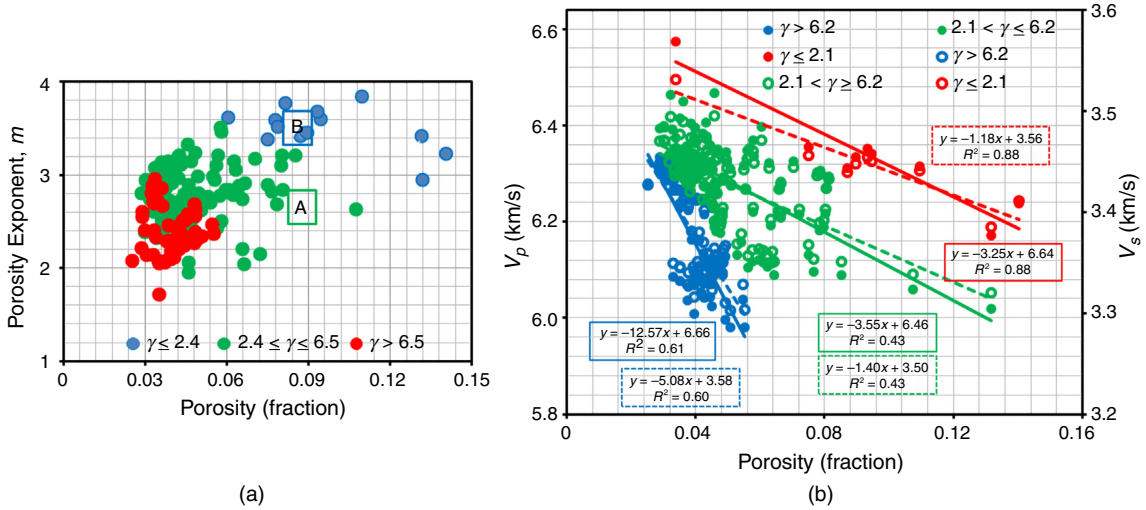

Fig. 5—Crossplot of total porosity vs. porosity exponent (m) and velocities (V_p and V_s). The scattering points are colored with the frame-flexibility-factor values, and this results in (a) distinct dispersed clusters and (b) trends. The variations of m and velocities with the pore-type mixing can be shown with the frame-flexibility factor (γ). Points *A* and *B* show how the porosity exponent varies with the pore-type composition; there is a difference of nearly unity (approximately 0.83) at a porosity of approximately 7.9%. Their relative pore-type mixtures are shown in Track 4 in Fig. 3.

Although the rock frame-flexibility factor (γ) has enabled the grouping of the scattering points into distinct clusters, its application has not led to defining consistent ϕ/m relationships (trends), which can be applied to predict m. This can suggest that there is no direct correlation between the porosity exponent m and rock velocities (V_p and V_s), although they both vary strongly with the pore-structure types in carbonates, rather than the bulk porosity itself (Sun 2000, 2004; Dou et al. 2011). However, it can be noted that the results clearly show that the rock-frame-flexibility factor can allow establishing of consistent porosity/velocity relationships (Fig. 5b). This observation can suggest that further work is needed to redefine γ for its application to establish consistent ϕ/m relationships. This will be the subject of future research.

Discussion

In this study, a quadruple-porosity model was proposed for accurate determination of the porosity exponent m in naturally fractured vuggy reservoirs in which the porosity system can comprise four pore-type classes, such as ϕ_b, CVGs, NFs, and SVGs, existing in any possible combination. The model was validated using water-saturation estimates, which vary strongly with the porosity exponent m in such a multiporosity reservoir. **Table 3** shows some computed statistical parameters used to determine the model-prediction accuracy, compared with the triple-porosity models, namely the Aguilera and Aguilera (2004) and Al-Ghamdi et al. (2011) models. The results demonstrate that there is much closer proximity between the laboratory values and the predicted values obtained with the model proposed in this study, as indicated by the mean absolute percentage error of 8.9%, and the mean-residual (MR) value of nearly zero. The parameter MR quantifies the departure of predicted from actual values. If compared with those obtained with the triple-porosity models herein considered, these values are the smallest (Table 3). It can be concluded that the proposed quadruple porosity can ensure better estimation of water saturation, and hence accurate hydrocarbon-volume quantification, compared with the triple-porosity models.

	S_w (m_1)	S_w (m_2)	S_w (m_3)	S_w (m_4)	S_w (m_5)
MR	0.21	–0.03	0.22	–0.02	–0.01
MAPE	46.0	10.4	46.8	10.0	8.9

Table 3—Statistical parameters computed using data from Table 2. MAPE = mean absolute percentage error.

Furthermore, considering the presented data for numerical applications of the triple-porosity model and improved triple-porosity models [Table 1 in both Aguilera and Aguilera (2004) and Al-Ghamdi et al. (2011)], it is apparent that the amounts of the touching-vug porosity are low enough, and thus likely less representative of common naturally fractured vuggy reservoirs. This was actually partially the reason for postulating the two hypotheses to test the applicability of these models in naturally fractured vuggy reservoirs that have high-enough CVG porosity, such as Tahe Oilfield Ordovician carbonate reservoirs. For each hypothesis, the S_w obtained with the triple-porosity model and improved triple-porosity model are approximately equal, and this can indicate that the two models have practically similar prediction ability. However, the results in Table 3 and **Fig. 6** show there is a good correlation between the actual and the predicted values with the second hypothesis ($\phi_2 =$ NF), as shown by the coefficients of determination ($R^2 = 0.9$, blue and red boxes,), MR (approximately 0.03), and mean absolute percentage error (approximately 10%). Conversely, for the first hypothesis ($\phi_2 =$ NFs±CVGs) to reproduce the two triple-porosity models, the results indicate a poor correlation between the predicted and the actual values. The data are highly scattered (Fig. 6), and the mean absolute percentage error (46%) and MR (approximately 0.22) are very significant. Therefore, this can suggest that the two triple-porosity models are not suitable for typical reservoirs according to the first hypothesis, whereas the second hypothesis can clearly recast their suitability for naturally fractured vuggy reservoirs with low values of CVGs (caves, cavernous, and so forth).

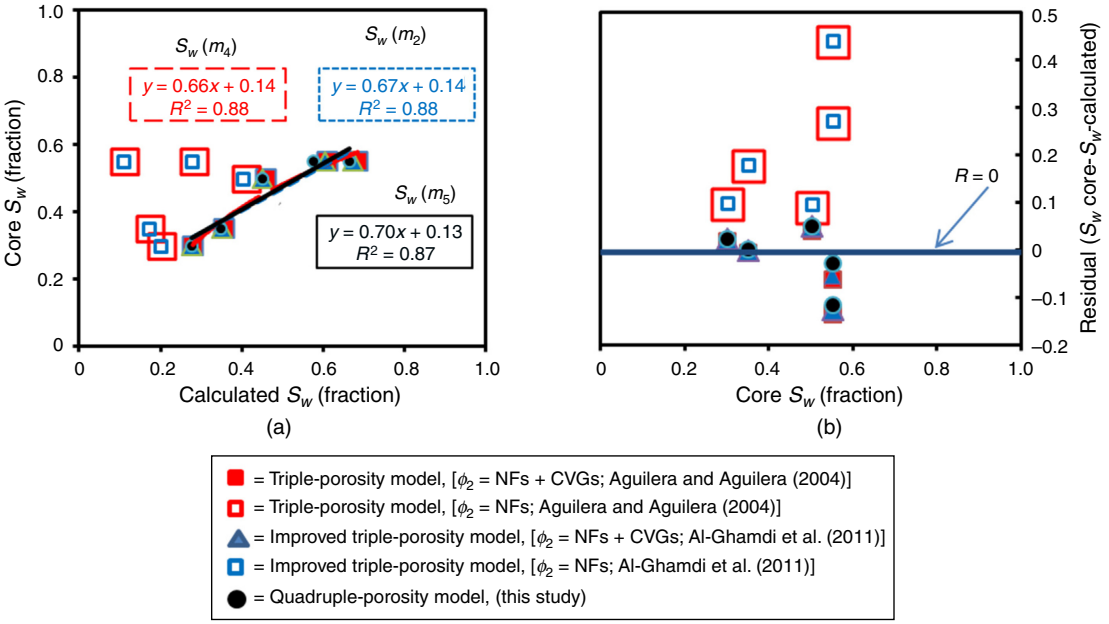

Fig. 6—Computation of water saturation for the model validation using the data given in Table 3. (a) Comparison of water saturation as calculated with the different models and laboratory core water saturation. The results show that the data computed with the two triple-porosity models deviate from the 1:1 trendline, compared with the proposed quadruple-porosity model and the reformulated triple-porosity models showing a good comparison ($R^2 = 0.9$). (b) Residual values vs. laboratory core water-saturation estimates. The residual value is determined as the difference between the core measured value and the calculated value. Again, the two triple-porosity models show high positive residuals, and the proposed quadruple-porosity model and the reformulated triple-porosity models show less departure from the zero residual line ($R = 0$, blue line).

Moreover, the results show that triple-porosity models fail to meet the standard for certain combinations of the four pore-type classes (ϕ_m, CVGs, NFs, and SVGs). In addition, the results suggest that the triple-porosity model and improved triple-porosity model attached more weight to the CVGs in influencing the variations of m because a low-moderate fraction of CVGs can cause a substantial decrease in m ($<m_b$) even if SVGs are prevalent, which led to an underestimation of S_w. This observation was also previously demonstrated with the dual/triple modeling in Berg (2006). The author argued that this likely relates to an improper scaling of the CVGs and/or unbalancing of the triple-porosity models, and thus the need for improved models, such as the proposed quadruple-porosity model.

In addition, the results show that m varies with the porosity systems, and specific pore type and its abundance (Ragland 2002), and also m relates poorly to the bulk porosity and any porosity range as well. On the basis of total porosity-based empirical relationships in multiporosity reservoirs, such as the Tahe Oilfield Ordovician carbonate reservoirs, this can preclude its prediction. This situation is different from several studies in the literature in different carbonate reservoirs, such as Ellenburger dolomite in west Texas, the Delaware Basin (Neustaedter 1968), offshore Abu Dhabi (Borai, 1987), Focke and Munn (1987), and Iranian reservoirs (Hasanigiv and Rahimi 2008). It is suspected that this difference could possibly be associated with the influence of the deep burial diagenesis that has resulted in significant modification of the pore space in the studied reservoirs, which mostly comprises secondary pore types.

Conclusions

The quadruple-porosity model was proposed to accurately account for the variance of porosity exponent m with fracture and CVG porosities separately, in addition to the matrix and SVG porosities. The model appears well-structured because it enables more accurate determination of m, compared with triple-porosity models. Correspondingly, it allows more accurate water-saturation calculations, and thus reliable estimation of hydrocarbon reserves. The study has shown that the triple-porosity model and improved triple-porosity model are highly sensitive to the abundance of CVGs and result in the underestimation of water saturation. In addition, the findings suggest that the triple-porosity models (Aguilera and Aguilera 2004) and improved triple-porosity models (Al-Ghamdi et al. 2011) are well-suited for reservoirs with essentially the combination of the matrix, fracture, and SVG (nonconnected) porosities.

Taking into account the difficulties associated with the partition of the total porosity into different porosity fractions, and the availability of necessary data, new m/ϕ correlations that consider the pore-type mixing and abundance of any occurring pore type were

established, with coefficients of determination from 0.7 to 0.9. These correlations can be applied using a detailed description of pore systems from the core and/or the thin section.

Nomenclature

a = constant in formation-factor equation, dimensionless
A = cross-sectional area, L^2, m^2; see Fig. A-1a for A_1 and A_2
C = constant function of drilling-fluid properties (Overton and Lipson 1958), dimensionless
D_f = formation depth (continuous)
F = formation (resistivity) factor, particularly of the matrix system at reservoir temperature when it is 100% saturated with water of resistivity R_w, Ω·m, dimensionless
F_{sys} = formation factor of the composite system
K = electrochemical spontaneous potential coefficient (Eq. B-3)
L = length, m (see Fig. A-1a for L_c, L_{nc}, and L_{12})
m = quadruple/triple/dual porosity exponent for the reservoir, dimensionless, as given in Table 2 (see Table 2 for m_1 through m_5)
m_b = porosity exponent of the matrix block attached only to the matrix system
m_f = porosity exponent of the NFs (assumed to be equal to 1.0 in this paper)
m_v = porosity exponent of the vugs (Berg 2006)
n = water-saturation exponent, dimensionless
R_c = resistivity of the CVGs at reservoir temperature when it is 100% saturated with water of resistivity R_w, Ω·m
R_m = mud resistivity at formation temperature, Ω·m
R_{mf} = mud-filtrate resistivity at reservoir temperature, Ω·m
R_{mfe} = equivalent mud-filtrate resistivity at reservoir temperature, Ω·m
R_{nc} = resistivity of the nonconnected vugs at reservoir temperature when it is 100% saturated with water of resistivity R_w, Ω·m
R_o = resistivity of the matrix system at reservoir temperature when it is 100% saturated with water of resistivity R_w, Ω·m
R_{sys} = resistivity of the composite (quadruple-porosity) system at reservoir temperature when it is 100% saturated with water of resistivity R_w, Ω·m
R_t = true resistivity of the composite system, Ω·m
R_w = water resistivity at reservoir temperature, Ω·m
R_{we} = equivalent formation-water resistivity at reservoir temperature, Ω·m
R_1 = resistivity of the matrix system at reservoir temperature when it is 100% saturated with water of resistivity R_w, as defined in Appendix A, Ω·m
R_2 = resistivity of the NFs at reservoir temperature when it is 100% saturated with water of resistivity R_w, as defined in Appendix A, Ω·m
R_{12} = resistivity of a system made out of matrix and fractures at reservoir temperature when it is 100% saturated with water of resistivity R_w, Ω·m
R^2 = coefficient of determination
S_w = water saturation of the composite system, fraction
SP = spontaneous potential, mV
T = temperature,°C
T_f = formation temperature,°C
T_s = surface temperature,°C
V = volume of the system (i.e., total or bulk volume of the system; Fig. A-1a), fraction
V_c = volume of the CVGs attached to the bulk volume of the system, fraction (Fig. A-1a, V_3)
V_f = volume of the fractures attached to the bulk volume of the system, fraction (Fig. A-1a, V_2)
V_m = volume of the matrix porosity attached to the matrix system, fraction (Fig. A-1a)
V_{nc} = volume of the nonconnected vugs attached to the bulk volume of the system, fraction (Fig. A-1a, V_4)
V_r = volume of the rock grains in the system (Fig. A-1a)
V_1 = volume of the matrix system attached to the bulk volume of the system (Fig. A-1a)
V_{12} = volume of the matrix system and fractures attached to the bulk volume of the system, fraction (Fig. A-1a)
V_{34} = volume of the SVGs and CVGs attached to the bulk volume of the system, fraction (Fig. A-1a)
γ = rock-frame-flexibility factor (Sun 2000)
ΔT = geothermal gradient,°C/km
μMo = micromoldic separate-vug porosity
ν = partitioning coefficient = ϕ_2/ϕ, fraction
ν_{nc} = nonconnected-vug porosity ratio = ϕ_{nc}/ϕ, fraction (Lucia 1983)
ρ = density, g/cm^3
ρ_b = bulk density, g/cm^3
ρ_f = fluid density, g/cm^3
ρ_m = mud density, g/cm^3
ρ_{ma} = matrix density, g/cm^3
ϕ = total porosity, fraction, percentage
ϕ_b = matrix-block porosity attached to the bulk volume of the matrix system; equivalent to porosity from unfractured plugs, fraction
ϕ_{cv} = porosity of CVGs attached to the bulk volume of the system as shown in Appendix A, fraction (Fig. A-1b)
ϕ_f = porosity of NFs attached to bulk volume of the system, ϕ_2, fraction
ϕ_m = matrix-block porosity attached to the bulk volume of the composite system as shown in Appendix A (Fig. A-1), fraction
ϕ_{nc} = porosity of nonconnected vugs attached to the bulk volume of the system as given in Appendix A, fraction
ϕ_2 = porosity of NFs attached to bulk volume of the system, fraction

Acknowledgments

This work was supported by National Key Research and Development Program of China (Grant No. 2017YFC0603104), China Scholarship Council (Grant No. 2015563007), and Ministère de l'Enseignement Supérieur, de la Recherche et de l'Innovation, Agence Nigérienne des Allocations et des Bourses. The technical support from SINOPEC is greatly acknowledged.

References

Abdassah, D. and Ershaghi, I. 1986. Triple-Porosity Systems for Representing Naturally Fractured Reservoirs. *SPE Form Eval* **1** (2): 113–127. SPE-13409-PA. https://doi.org/10.2118/13409-PA.

Adisoemarta, P. S., Anderson, G. A., Frailey, S. M. et al. 2000. Historical Use of *m* and *a* in Well Log Interpretation: Is Conventional Wisdom Backwards? Paper presented at the SPE Permian Basin Oil and Gas Recovery Conference, Midland, Texas, USA, 21–23 March. SPE-59699-MS. https://doi.org/10.2118/59699-MS.

Aguilera, C. G. and Aguilera, R. 2009. Effect of Fracture Dip on Petrophysical Evaluation of Naturally Fractured Reservoirs. *J Can Pet Technol* **48** (7): 25–29. PETSOC-09-07-25. https://doi.org/10.2118/09-07-25.

Aguilera, M. S. and Aguilera, R. 2003. Improved Models for Petrophysical Analysis of Dual Porosity Reservoirs. *Petrophysics* **44** (1): 21–35. SPWLA-2003-v44n1a1.

Aguilera, R. 1976. Analysis of Naturally Fractured Reservoirs from Conventional Well Logs (includes associated papers 6420 and 6421). *J Pet Technol* **28** (7): 764–772. SPE-5342-PA. https://doi.org/10.2118/5342-PA.

Aguilera, R. 2010. Effect of Fracture Dip and Fracture Tortuosity on Petrophysical Evaluation of Naturally Fractured Reservoirs. *J Can Pet Technol* **49** (9): 69–76. SPE-139847-PA. https://doi.org/10.2118/139847-PA.

Aguilera, R. F. and Aguilera, R. 2004. A Triple Porosity Model for Petrophysical Analysis of Naturally Fractured Reservoir. *Petrophysics* **45** (2): 157–166. SPWLA-2004-V45N2A4.

Al-Ghamdi, A., Chen, B., Behmanesh, H. et al. 2011. An Improved Triple-Porosity Model for Evaluation of Naturally Fractured Reservoirs. *SPE Res Eval & Eng* **14** (4): 397–404. SPE-132879-PA. https://doi.org/10.2118/132879-PA.

Ali, M. T., Ezzat, A. A., and Nasr-El-Din, H. A. 2020. A Model To Simulate Matrix-Acid Stimulation for Wells in Dolomite Reservoirs with Vugs and Natural Fractures. *SPE J*. **25** (2): 609–631. SPE-199341-PA. https://doi.org/10.2118/199341-PA.

Amyx, J. W., Bass, D. M. Jr., and Whiting, R. L. 1960. *Petroleum Reservoir Engineering*. New York, New York, USA: McGraw-Hill.

Anselmetti, F. S., Luthi, S., and Eberli, G. P. 1998. Quantitative Characterization of Carbonate Pore Systems by Digital Image Analysis. *AAPG Bull* **82** (10): 1815–1836.

Archie, G. E. 1942. The Electrical Resistivity Log as an Aid in Determining Some Reservoir Characteristics. In *Transactions of the Society of Petroleum Engineers*, Vol. 146, Part I, SPE-942054-G, 54–62. Richardson, Texas, USA: Society of Petroleum Engineers.

Arps, J. J. 1953. The Effect of Temperature on the Electrical Resistivity of Sodium Chloride Solutions. *J Pet Technol* **5** (10): 17–20. SPE-953327-G. https://doi.org/10.2118/953327-G.

Bahrami, F., Moussavi-Harami, R., Khanehbad, M. et al. 2017. Identification of Pore Types and Pore Facies for Evaluating the Diagenetic Performance on Reservoir Quality: A Case Study from the Asmari Formation in Ramin Oil Field, SW Iran. *Geosci J* **21** (4): 565–577. https://doi.org/10.1007/s12303-016-0014-0.

Bateman, R. M. and Konen, C. E. 1977. The Log Analyst and the Programmable Pocket Calculator. *The Log Analyst* **18** (5): 3–10. SPWLA-1977-vXVIIIn5a1.

Berg, C. R. 2006. Dual-Porosity Equations from Effective Medium Theory. Paper presented at the SPE Annual Technical Conference and Exhibition, San Antonio, Texas, USA, 24–27 September. SPE-101698-MS. https://doi.org/10.2118/101698-MS.

Berryman, J. G. 1995. Mixture Theories for Rock Properties. In *Global Earth Physics: A Handbook of Physical Constants*, ed. T. J. Ahrens, 205–228. Washington, DC, USA: AGU Reference Shelf Series, America Geophysical Union.

Borai, A. M. 1987. A New Correlation for the Cementation Factor in Low-Porosity Carbonates. *SPE Form Eval* **2** (4): 495–499. SPE-14401-PA. https://doi.org/10.2118/14401-PA.

Borai, A. M. 1990. Log Interpretation of Low Porosity Carbonates. SPE-21316-MS. https://doi.org/10.2118/21316-MS.

Byrnes, A. P., Cluff, R., and Webb, J. 2006. Analysis of Critical Permeability, Capillary Pressure, and Electrical Properties for Mesaverde Tight-Gas Sandstones From Western U.S. Basins. Quarterly Technical Progress Report, DOE Contract No. DE-FC26-05NT43660, University of Kansas Center for Research, Lawrence, Kansas, USA. https://doi.org/10.2172/971248.

Carothers, J. E. 1968. A Statistical Study of the Formation Factor Relation to Porosity. *The Log Analyst* **9:** 38–52.

CPI SY/T5336-2006, Professional Standard for Practices for Core Analysis. 2007. Beijing, China: Chinese Petroleum Industry.

Dou, Q., Sun, Y., and Sullivan, C. 2011. Rock-Physics-Based Carbonate Pore Type Characterization and Reservoir Permeability Heterogeneity Evaluation, Upper San Andres Reservoir, Permian Basin, West Texas. *J Appl Geophy* **74** (1): 8–18. https://doi.org/10.1016/j.jappgeo.2011.02.010.

Ehrlich, R., Crabtree, S. J., Horkowitz, K. O. et al. 1991. Petrophysical and Reservoir Physics I: Objective Classification of Reservoir Porosity. *AAPG Bull* **75** (10): 1547–1562. https://doi.org/10.1306/0C9B2989-1710-11D7-8645000102C1865D.

Feng, C.-G., Liu, S.-W., Wang, L.-S. et al. 2009. Present-Day Geothermal Regime in Tarim Basin, Northwest China: *Chinese J Geophys* **52** (6): 1237–1250. https://doi.org/10.1002/cjg2.1450.

Focke, J. W. and Munn, D. 1987. Cementation Exponents in Middle Eastern Carbonate Reservoirs. *SPE Form Eval* **2** (2): 155–167. SPE-13735-PA. https://doi.org/10.2118/13735-PA.

Fricke, H. 1924. A Mathematical Treatment of the Electric Conductivity and Capacity of Disperse Systems. I. The Electric Conductivity of a Suspension of Homogeneous Spheroids. *Phys Rev* **24** (5): 575–587. https://doi.org/10.1103/PhysRev.24.575.

Gharechelou, S., Daraei, M., and Amini, A. 2016. Pore Types Distribution and Their Reservoir Properties in the Sequence Stratigraphic Framework: A Case Study from the Oligo-Miocene Asmari Formation, SW Iran. *Arab J Geosci* **9** (3): 194–213. https://doi.org/10.1007/s12517-015-2141-8.

Haro, C. F. 2006. Permeability Modeling. Setting Archie and Carman-Kozeny Right. Paper presented at the SPE Europec/EAGE Annual Conference and Exhibition, Vienna, Austria, 15–16 June. SPE-100200-MS. https://doi.org/10.2118/100200-MS.

Haro, C. F. 2010. The Equations Archie Forgot, Anisotropy of the Rocks. *SPE Res Eval & Eng* **13** (5): 823–836. SPE-123913-PA. https://doi.org/10.2118/123913-PA.

Hassanzadeh Azar, J., Javaherian, A., Pishvaie, M. R. et al. 2008. An Approach to Defining Tortuosity and Cementation Factor in Carbonate Reservoir Rocks. *J Pet Sci Eng* **60** (2): 125–131. https://doi.org/10.1016/j.petrol.2007.05.010.

Hasanigiv, M. and Rahimi, M. 2008. New Correlations for Porosity Exponent in Carbonate Reservoirs of Iranian Oil Fields in Zagros Basin. *JSUT* **34** (2): 1–7.

Hilchie, D. W. 1978. *Applied Openhole Log Interpretation for Geologists and Petroleum Engineers*. Golden, Colorado, USA: D. W. Hilchie.

Huang, Q., Dou, Q., and Sun, Y. 2017. Characterization of Pore Structure Variation and Permeability Heterogeneity in Carbonate Rocks Using MICP and Sonic Logs: Puguang Gas Field, China. *Petrophysics* **58** (6): 576–591. SPWLA-2017-v58n6a2.

Issoufou Aboubacar, M. S., Zhongxian, C., Boukari, I. O. et al. *In press*. New Vuggy Porosity Models-Based Interpretation Methodology for Reliable Pore System Characterization, Ordovician Carbonate Reservoirs in Tahe Oilfield, North Tarim Basin. *J Pet Sci Eng* (submitted 04 February 2020).

Iwere, F. O., Moreno, J. E., Apaydin, O. G. et al. 2002. Vug Characterization and Pore Volume Compressibility for Numerical Simulation of Vuggy and Fractured Carbonate Reservoirs. Paper presented at the SPE International Petroleum Engineering Conference, Villahermosa, Mexico, 10–12 February. SPE-74341-MS. https://doi.org/10.2118/74341-MS.

Jorgensen, D. G. 1988. Using Geophysical Logs To Estimate Porosity, Water Resistivity, and Intrinsic Permeability. USGS Water-Supply Paper 2321, US Geological Survey, US Department of the Interior, Denver, Colorado, USA.

Kuster, G. T. and Toksöz, M. N. 1974. Velocity and Attenuation of Seismic Waves in Two-Phase Media: Part I, Theoretical Formulations. *Geophysics* **39** (5): 587–606. https://doi.org/10.1190/1.1440450.

Li, B., Tan, X., Wang, F. et al. 2017. Fracture and Vug Characterization and Carbonate Rock Type Automatic Classification Using X-Ray CT Images. *J Pet Sci Eng* **153** (May): 88–96. https://doi.org/10.1016/j.petrol.2017.03.037.

Li, H. and Zhang, J. 2018. Well Log and Seismic Data Analysis for Complex Pore-Structure Carbonate Reservoir Using 3D Rock Physics Templates. *J Appl Geophys* **151** (April): 175–183. https://doi.org/10.1016/j.jappgeo.2018.02.017.

Li, X. Y., Qin, R. B., Mao, Z. Q. et al. 2013. Building a Computational Model of the Cementation Exponent for Complex Porous Reservoirs Based on the Maxwell Equations. *Petrophysics* **54** (4): 341–348. SPWLA-2013-v54n4-A2.

Lønøy, A. 2006. Making Sense of Carbonate Pore Systems. *AAPG Bull* **90** (9): 1381–1405. https://doi.org/10.1306/03130605104.

Lucia, F. J. 1983. Petrophysical Parameters Estimated from Visual Descriptions of Carbonate Rocks: A Field Classification of Carbonate Pore Space. *J Pet Technol* **35** (3): 629–637. SPE-10073-PA. https://doi.org/10.2118/10073-PA.

Lucia, F. J. 1995. Rock-Fabric/Petrophysical Classification of Carbonate Pore Space for Reservoir Characterization. *AAPG Bull*. **79** (9): 1275–1300.

Lucia, F. J. 2007. *Carbonate Reservoir Characterization: An Integrated Approach*, second edition. Berlin, Germany: Springer-Verlag.

Mahood, B. C. and Boyd, D. A. 1993. Formation Factor Relationships of Western Canada. Paper presented at the SPWLA 34th Annual Logging Symposium, Calgary, Alberta, Canada, 13–16 June. SPWLA-1993-FF.

Mavko, G. and Mukerji, T. 1995. Seismic Pore Space Compressibility and Gassmann's Relation. *Geophysics* **60** (6): 1743–1749. https://doi.org/10.1190/1.1443907.

Maxwell, J. C. 1954. *A Treatise on Electricity and Magnetism*, third edition. Mineola, New York, USA: Dover Books on Physics, Dover Publications.

Melani, L. H., Vidal, A. C., Filho, I. M. et al. 2015. The Impact of Archiés Parameters in the Calculation of Water Saturation for Carbonate Reservoir, Campos Basin, Brazil. *Proc.,* SEG Annual Meeting, New Orleans, Louisiana, USA, 18–23 October, 5634, SEG-2015-5915007. https://doi.org/10.1190/segam2015-5915007.1.

Meng, M., Fan, T., Duncan, I. J. et al. 2018. Characterization of Carbonate Microfacies and Reservoir Pore Types Based on Formation MicroImager Logging: A Case Study from the Ordovician in the Tahe Oilfield, Tarim Basin, China. *Interpretation* **6** (1): T71–T82. https://doi.org/10.1190/INT-2017-0043.1.

Montaron, B. 2009. Connectivity Theory–A New Approach to Modeling Non-Archie Rocks. *Petrophysics* **50** (2): 102–115. SPWLA-2009-v50n2a2.

Morgan, J. T. and Gordon, D. T. 1970. Influence of Pore Geometry on Water-Oil Relative Permeability. *J Pet Technol* **22** (10): 1199–1208. SPE-2588-PA. https://doi.org/10.2118/2588-PA.

Müller-Huber, E. and Schön, J. 2013. A Modified Archie Relationship—A Novel Approach To Evaluate Carbonate Reservoirs with Regard to Fracture and Isolated Vuggy Porosity for $S_w = 1$. Paper presented at the International Petroleum Technology Conference, Beijing, China, 26–28 March. IPTC-16695-MS. https://doi.org/10.2523/IPTC-16695-MS.

Myers, M. T. 1991. Pore Combination Modeling: A Technique for Modeling the Permeability and Resistivity Properties of Complex Pore Systems. Paper presented at the SPE Annual Technical Conference and Exhibition, Dallas, Texas, USA, 6–9 October. SPE-22662-MS. https://doi.org/10.2118/22662-MS.

Nair, N. G., Bryant, S. L., and Jennings, J. W. 2008. Finding the Continuum Scale in Highly Heterogeneous Rocks: Example of a Large Touching Vug Carbonate. Paper presented at the SPE Annual Technical Conference and Exhibition, Denver, Colorado, USA, 21–24 September. SPE-115347-MS. https://doi.org/10.2118/115347-MS.

Neustaedter, P. R. H. 1968. Log Evaluation of Deep Ellenburger Gas Zones. Paper presented at the SPE Deep Drilling and Development Symposium, Monahans, Texas, USA, 28 March. SPE-2071-MS. https://doi.org/10.2118/2071-MS.

Ning, C. Z. 2017. Control of Stratigraphic Sequence on Karst Reservoirs: A Case Study on the Reservoirs in the North Tarim Basin, China. Oral presentation of Search and Discovery Article 10936 given at the AAPG Annual Convention and Exhibition, Houston, Texas, USA, 2–5 April.

Olusola, B. K., Yu, G., and Aguilera, R. 2013. The Use of Electromagnetic Mixing Rules for Petrophysical Evaluation of Dual-and Triple-Porosity Reservoirs. *SPE Res Eval & Eng* **16** (4): 378–389. SPE-162772-PA. https://doi.org/10.2118/162772-PA.

Overton, H. L. and Lipson, L. B. 1958. A Correlation of the Electrical Properties of Drilling Fluids with Solids Content. In *Transactions of the Society of Petroleum Engineers,* Vol. 213, Part I, SPE-1171-G, 333–336. Richardson, Texas, USA: Society of Petroleum Engineers.

Pérez-Rosales, C. and Luna, E. 2004. Characterization of Vuggy Fractured Media: A Practical Approach. Paper presented at the SPE International Petroleum Engineering Conference, Puebla, Mexico, 8–9 November. SPE-91863-MS. https://doi.org/10.2118/91863-MS.

Pérez-Rosales, C. and Luna, E. E. 2005. Naturally Fractured Reservoirs: How To Estimate Secondary Porosity. Paper presented at the SPE Latin and Caribbean Petroleum Engineering Conference, Rio de Janeiro, Brazil, 20–23 June. SPE-94525-MS. https://doi.org/10.2118/94525-MS.

Piedrahita, J. and Aguilera, R. 2017. A Petrophysical Dual-Porosity Model for Evaluation of Secondary Mineralization and Tortuosity in Naturally Fractured Reservoirs. *SPE Res Eval & Eng* **20** (2): 304–316. SPE-180242-PA. https://doi.org/10.2118/180242-PA.

Pirson, S. J. 1957. Log Interpretation in Rocks with Multiple Porosity Types–Water or Oil Wet. *World Oil* **June**: 196.

Porter, C. R. and Carothers, J. E. 1970. Formation Factor-Porosity Relation from Well Log Data. Paper presented at the SPWLA 11th Annual Logging Symposium, Los Angeles, California, USA, 3–6 May. SPWLA-1970-A.

Qin, Z., Pan, H., Ma, H. et al. 2016. Fast Prediction Method of Archie's Cementation Exponent. *J Nat Gas Sci Eng* **34** (July): 291–297. https://doi.org/10.1016/j.jngse.2016.06.070.

Ragland, D. A. 2002. Trends in Cementation Exponents (m) for Carbonate Pore Systems. *Petrophysics* **43** (5): 434–446. SPWLA-2002-v43n5a4.

Raiga-Clemenceau, J. 1977. The Cementation Exponent in the Formation Factor–Porosity Relation: The Effect of Permeability. Paper presented at the SPWLA 18th Annual Logging Symposium, Houston, Texas, USA, 5–8 June. SPWLA-1977-R.

Ramamoorthy, R., Ramakrishnan, T. S., Dasgupta, S. et al. 2019. Towards a Petrophysically Consistent Implementation of Archie's Equation for Heterogeneous Carbonate Rocks. Paper presented at the SPWLA 60th Annual Logging Symposium, The Woodlands, Texas, USA, 15–19 June. SPWLA-2019-P.

Rasmus, J. C. 1983. A Variable Cementation Exponent, M, for Fractured Carbonates. *The Log Analyst* **24** (6): 13–23. SPWLA-1983-vXXIVn6a2.

Rezaee, M. R., Motiei, H., and Kazemzadeh, E. 2007. A New Method To Acquire m Exponent and Tortuosity Factor for Microscopically Heterogeneous Carbonates. *J Pet Sci Eng* **56** (4): 241–251. https://doi.org/10.1016/j.petrol.2006.09.004.

Sadeghnejad, S. and Gostick, J. 2020. Multiscale Reconstruction of Vuggy Carbonates by Pore-Network Modeling and Image-Based Technique. *SPE J*. **25** (1): 253–267. SPE-198902-PA. https://doi.org/10.2118/198902-PA.

Saleh, A. A. and Castagna, J. P. 2004. Revisiting the Wyllie Time Average Equation in the Case of Near-Spherical Pores. *Geophysics* **69** (1): 45–55. https://doi.org/10.1190/1.1649374.

Sayers, C. M. 2008. The Elastic Properties of Carbonates. *Lead Edge* **27** (8): 1020–1024. https://doi.org/10.1190/1.2967555.

Schlumberger. 2009. *Log Interpretation Charts*, second edition. Sugar Land, Texas, USA: Schlumberger.

Serra, O. 1989. *Schlumberger Formation MicroScanner Image Interpretation*. Houston, Texas, USA: Schlumberger Educational Services.

Sihvola, A. 1999. *Electromagnetic Mixing Formulas and Applications*. London, UK: Institute of Electrical Engineers.

Smith, L. B., Eberli, G. P., Masaferro, J. L. et al. 2003. Discrimination of Effective from Ineffective Porosity in Heterogeneous Cretaceous Carbonates, Al-Ghubar Field, Oman. *AAPG Bull* **87** (9): 1509–1529. https://doi.org/10.1306/041703200180.

Soto, J. O., Soto, D. O., and Soto, R. B. 2015. A New Reservoir Classification Based on Pore Types Improves Characterization—Part B. Paper presented at the SPE Latin American and Caribbean Petroleum Engineering Conference, Quito, Ecuador, 18–20 November. SPE-117237-MS. https://doi.org/10.2118/117237-MS.

Sun, S. Z., Wang, H., Liu, Z. et al. 2012. The Theory and Application of DEM-Gassmann Rock Physics Model for Complex Carbonate Reservoirs. *Lead Edge* **31** (2): 152–158. https://doi.org/10.1190/1.3686912.

Sun, Y. F. 2000. Core-Log-Seismic Integration in Hemipelagic Marine Sediments on the Eastern Flank of the Juan De Fuca Ridge. In *Proceedings of the Ocean Drilling Program, Scientific Results*, ed. A. Fisher, E. E. Davis, C. Escutia, Vol. 168, 21–35. College Station, Texas, USA: Texas A&M University.

Sun, Y. F. 2004. Effects of Pore Structure on Elastic Wave Propagation in Rocks, AVO Modeling. *J Geophys Eng* **1** (4): 268–276. https://doi.org/10.1088/1742-2132/1/4/005.

Tabibi, M. and Emadi, M. A. 2003. Variable Cementation Factor Determination (Empirical Methods). Paper presented at the Middle East Oil Show, Bahrain, 9–12 June. SPE-81485-MS. https://doi.org/10.2118/81485-MS.

Tiab, D. and Donaldson, E. C. 2004. *Petrophysics: Theory and Practice of Measuring Reservoir Rock and Fluid Transport Properties*, second edition. Amsterdam, The Netherlands: Elsevier.

Towle, G. 1962. An Analysis of the Formation Resistivity Factor-Porosity Relationship of Some Assumed Pore Geometries. Paper presented at the SPWLA 3rd Annual Logging Symposium, Houston, Texas, USA, 17–18 May. SPWLA-1962-C.

Wang, F. P. and Lucia, F. J. 1993. Comparison of Empirical Models for Calculating the Vuggy Porosity and Cementation Exponent of Carbonates from Log Responses. Geological Circular 93-4, Bureau of Economic Geology, University of Texas at Austin, Austin, Texas, USA.

Wang, H. 2017. Improved Dual-Porosity Models for Petrophysical Analysis of Vuggy Reservoirs. *J Geophys Eng* **14** (4): 758–768. https://doi.org/10.1088/1742-2140/aa6989.

Watfa, M. and Nurmi, R. 1987. Calculation of Saturation, Secondary Porosity and Producibility in Complex Middle East Carbonate Reservoirs. Paper presented at the SPWLA 28th Annual Logging Symposium, London, UK, 29 June–2 July. SPWLA-1987-CC.

Winsauer, W. O., Shearin, H. M. Jr., Masson, P. H. et al. 1952. Resistivity of Brine-Saturated Sands in Relation to Pore Geometry. *AAPG Bull* **36** (2): 253–277. https://doi.org/10.1306/3D9343F4-16B1-11D7-8645000102C1865D.

Wyllie, M. R. J. and Gregory, A. R. 1953. Formation Factors of Unconsolidated Porous Medium: Influence of Practical Shale and Effect of Cementation. *J Pet Technol* **5** (4): 103–110. SPE-223-G. https://doi.org/10.2118/223-G.

Wyllie, M. R. J., Gregory, A. R., and Gardner, L. W. 1958. An Experimental Investigation of Factors Affecting Elastic Wave Velocities in Porous Media. *Geophysics* **23** (3): 459–493. https://doi.org/10.1190/1.1438493.

Xu, S. and Payne, M. A. 2009. Modeling Elastic Properties in Carbonate Rocks. *Lead Edge* **28** (1): 66–74. https://doi.org/10.1190/1.3064148.

Xu, S. and White, R. E. 1996. A Physical Model for Shear-Wave Velocity Prediction. *Geophys Prospect* **44** (4): 687–717. https://doi.org/10.1111/j.1365-2478.1996.tb00170.x.

Appendix A—Development of the Quadruple-Porosity Model

The model was developed using the assumption that a reservoir can have four pore types, such as matrix, NFs, SVGs, and CVGs. The reservoir rock is volumetrically assumed to be a two-component system: the insulating solid matrix and the conductive void space, ϕ. The latter that is defined in proportion of the rock bulk volume comprises several components, the fractions of which can also be established in proportion of the rock bulk volume, and subsequently normalized to ϕ **(Fig. A-1a).** For simplicity, the modeling was conducted using the electric-resistance-network concept in literature (Serra 1989; Aguilera and Aguilera 2003), as shown in Fig. A-1b.

First, we apply a parallel resistance network between the matrix ($R_1 = R_o$) and fractures ($R_2 = R_w$) (Fig. A-1),

$$\frac{1}{r_{12}} = \frac{1}{r_1} + \frac{1}{\mathrm{r}_2}, \qquad \text{(A-1)}$$

where

$$r_{12} = R_{12}\frac{L_{12}}{A}, \quad r_1 = R_o\frac{L_{12}}{A_1}, \quad r_2 = R_w\frac{L_{12}}{A_2}. \qquad \text{(A-2)}$$

Inserting Eq. A-2 into Eq. A-1 gives

$$\frac{A}{R_{12}L_{12}} = \frac{A_1}{R_oL_{12}} + \frac{A_2}{R_wL_{12}} \rightarrow \frac{AL_{12}}{R_{12}} = \frac{A_1L_{12}}{R_o} + \frac{A_2L_{12}}{R_w}. \qquad \text{(A-3)}$$

Volumes of the system can be defined as

$$\begin{aligned}
&V_{12} = V_r + V_m + V_2 = V - V_{34} = AL_{12},\\
&V_1 = V_r + V_m = V_{12} - V_2 = A_1L_{12},\\
&V_2 = A_2L_{12},\\
&V_{34} = V_3 + V_4,\\
&V_3 = AL_c,\\
&V_4 = AL_{nc},\\
&V = V_{12} + V_{34} = AL. \qquad \text{(A-4)}
\end{aligned}$$

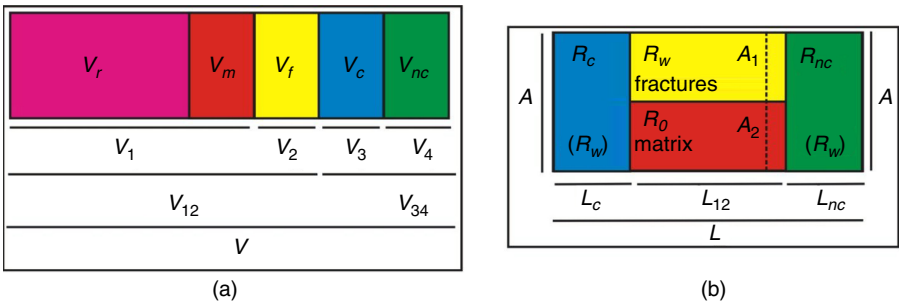

Fig. A-1—Conceptual diagram used to develop the quadruple-porosity model. (a) Schematic for representing the volumetric distribution of a naturally fractured vuggy reservoir rock made up of solid grains (V_r), matrix porosity (V_m), fractures (V_f), CVGs (V_c), and SVGs (V_{nc}). (b) Schematic for showing the matrix and fractures in parallel, and the combination of matrix and fractures in series with the SVGs and CVGs. Note that schematics are not scaled.

After dividing and multiplying by A and L_{12}, respectively, put the volume factors into Eq. A-3 to obtain

$$\frac{1}{R_{12}}=\frac{V_1/V_{12}}{R_o}+\frac{V_2/V_{12}}{R_w}. \quad \text{(A-5)}$$

The matrix, fracture, SVG, and CVG porosities can be defined as

$$\phi_m=\frac{V_m}{V},\quad \phi_b=\frac{V_m}{V_1},\quad \phi_2=\frac{V_2}{V},\quad \phi_c=\frac{V_3}{V},\quad \phi_{nc}=\frac{V_4}{V}. \quad \text{(A-6)}$$

From Eq. A-4,

$$V_{12}=V-V_{34}=V-(V\phi_c+V\phi_{nc})\rightarrow V_{12}=V(1-\phi_c-\phi_{nc}). \quad \text{(A-7)}$$

Expressing the numerators on the right-hand side of Eq. A-5 in terms of porosities,

$$\frac{V_2}{V_{12}}=\frac{\phi_2 V}{V(1-\phi_c-\phi_{nc})}=\frac{\phi_2}{1-\phi_c-\phi_{nc}}, \quad \text{(A-8)}$$

$$\frac{V_1}{V_{12}}=\frac{V_{12}-V_2}{V_{12}}=1-\frac{V_2}{V_{12}}=1-\frac{\phi_2}{1-\phi_c-\phi_{nc}}=\frac{1-\phi_c-\phi_{nc}-\phi_2}{1-\phi_c-\phi_{nc}}. \quad \text{(A-9)}$$

Inserting Eqs. A-8 and A-9 into Eq. A-5 and rearranging gives

$$\frac{1}{R_{12}}=\frac{1}{R_o}\left(\frac{1-\phi_c-\phi_{nc}-\phi_2}{1-\phi_c-\phi_{nc}}\right)+\frac{1}{R_w}\left(\frac{\phi_2}{1-\phi_c-\phi_{nc}}\right)\rightarrow R_{12}=\frac{R_oR_w(1-\phi_c-\phi_{nc})}{R_w(1-\phi_c-\phi_{nc}-\phi_2)+R_o\phi_2}. \quad \text{(A-10)}$$

Eq. A-10 is the resistivity of the matrix/fracture system in the quadruple-porosity model.

Next, apply the in-series resistance network for a system consisting of a matrix/fracture combination, CVGs ($R_3=R_c=R_w$), and SVGs ($R_4=R_{nc}=R_w$), as shown in Fig. A-1,

$$r_{sys}=r_{12}+r_c+r_{nc}=r_{12}+r_3+r_4, \quad \text{(A-11)}$$

where

$$r_{sys}=R_{sys}\frac{L}{A},\quad r_{12}=R_{12}\frac{L_{12}}{A},\quad r_c=R_c\frac{L_c}{A}=R_w\frac{L_c}{A},\quad r_{nc}=R_{nc}\frac{L_{nc}}{A}=R_w\frac{L_{nc}}{A}. \quad \text{(A-12)}$$

Inserting Eq. A-12 into Eq. A-11, and multiplying and dividing by A and L, respectively, gives

$$R_{sys}\frac{L}{A}=R_{12}\frac{L_{12}}{A}+R_w\frac{L_c}{A}+R_w\frac{L_{nc}}{A}\rightarrow R_{sys}=R_{12}\frac{AL_{12}}{AL}+R_w\frac{AL_c}{AL}+R_w\frac{AL_{nc}}{AL}. \quad \text{(A-13)}$$

Defining the R_{sys} in terms of volumes and porosities leads to

$$R_{sys}=R_{12}\frac{V_{12}}{V}+R_w\left(\frac{V_3}{V}+\frac{V_4}{V}\right)\rightarrow R_{sys}=R_{12}(1-\phi_c-\phi_{nc})+R_w(\phi_c+\phi_{nc}). \quad \text{(A-14)}$$

Inserting Eq. A-10 into Eq. A-14 gives

$$R_{sys}=R_w(\phi_c+\phi_{nc})+\frac{R_oR_w(1-\phi_c-\phi_{nc})^2}{R_w(1-\phi_c-\phi_{nc}-\phi_2)+R_o\phi_2}. \quad \text{(A-15)}$$

Writing the basic Archie equations for a system made of matrix (interparticle) porosity only,

$$R_o = FR_w, \quad \text{(A-16)}$$

$$F = \phi_b^{-m_b}. \quad \text{(A-17)}$$

Rewriting the basic Archie equations for a quadruple-porosity system made of matrix, fracture, CVG, and SVG porosities,

$$R_{\text{sys}} = F_{\text{sys}}R_w, \quad \text{(A-18)}$$

$$F_{\text{sys}} = \phi^{-m}. \quad \text{(A-19)}$$

After inserting Eq. A-19 into Eq. A-15, take R_o as a common factor of the second term of the right-hand side of Eq. A-15, cancel the R_w factor, and insert Eqs. A-16 and A-17 into Eq. A-20 to obtain the equation of the quadruple-porosity model (Eq. A-21).

$$F_{\text{sys}}R_w = R_w(\phi_c + \phi_{nc}) + \frac{R_w(1-\phi_c-\phi_{nc})^2}{\phi_2 + (1-\phi_c-\phi_{nc}-\phi_2)\dfrac{R_w}{R_o}}, \quad \text{(A-20)}$$

$$\phi^{-m} = (\phi_c + \phi_{nc}) + \frac{(1-\phi_c-\phi_{nc})^2}{\phi_2 + (1-\phi_c-\phi_{nc}-\phi_2)/\phi_b^{-m_b}}. \quad \text{(A-21)}$$

Writing the matrix porosity (ϕ_m) attached to the bulk volume of the composite system in terms of matrix porosity (ϕ_b) attached to the bulk volume of the matrix system, defining V_1 from Eq. A-6, expressing V in terms of volumes and matrix porosities, dividing by V and replacing the volumes by the porosity terms, and rearranging results in

$$V_m = \phi_b V_1 = \phi_m V \rightarrow V_1 = \frac{\phi_m V}{\phi_b}, \quad \text{(A-22)}$$

$$V = V_1 + V_2 + V_3 + V_4 \rightarrow V = \frac{\phi_m V}{\phi_b} + V_2 + V_3 + V_4, \quad \text{(A-23)}$$

$$\frac{V}{V} = \frac{\phi_m V}{\phi_b V} + \frac{V_2}{V} + \frac{V_3}{V} + \frac{V_4}{V} \rightarrow 1 = \frac{\phi_m}{\phi_b} + \phi_2 + \phi_c + \phi_{nc}, \quad \text{(A-24)}$$

$$\phi_m = \phi_b(1-\phi_2-\phi_c-\phi_{nc}). \quad \text{(A-25)}$$

The total porosity (ϕ) of the system can be given as

$$\phi = \phi_m + \phi_2 + \phi_c + \phi_{nc} = \phi b(1-\phi_2-\phi_c-\phi_{nc}) + \phi_2 + \phi_c + \phi_{nc}. \quad \text{(A-26)}$$

Isolating m (the porosity exponent of the quadruple-porosity system) and rearranging Eq. A-21 leads to

$$m = \frac{-\log\left[(\phi_c + \phi_{nc}) + \dfrac{(1-\phi_c-\phi_{nc})^2}{\phi_2 + (1-\phi_c-\phi_{nc}-\phi_2)/\phi_b^{-m_b}}\right]}{\log\phi}. \quad \text{(A-27)}$$

This is Eq. 1 presented in the text for estimating m for a reservoir characterized by a quadruple-porosity system. It can be expressed in terms of the vug-porosity ratio ($\nu_{nc} = \phi_{nc}/\phi$) (Lucia 1983) and the partitioning coefficient ($\nu = \phi_2/\phi$) (Aguilera and Aguilera 2003).

Appendix B—Determination of Water Saturation

The first step consists of determining reliable formation-water-resistivity (R_w) data that are required to ensure accurate water-saturation calculation from wireline logs, particularly using the Archie equation, Eq. B-1. As usual, we established an R_w/depth profile from a combination of the spontaneous-potential (SP) log and computed mud-filtrate-resistivity (R_{mf}) depth profile.

$$S_w = \sqrt[2]{\frac{R_w}{\phi^m \cdot R_t}}. \quad \text{(B-1)}$$

The R_{mf} depth-profile was herein inverted from actual drilling-mud properties, such as density (ρ_m) and resistivity (R_m). To do so, we applied the Overton and Lipson (1958) correlation, $R_{mf} = C(R_m)^{1.07}$, where the empirical factor C is mud-weight dependent. By crossplotting the data in Chart Gen-3 in Schlumberger (2009), it was found that the variation of C with the mud density can be better predicted with a power-law equation, $C = 1.0474(\rho_m)^{-1.556}$, and coefficient of determination $R^2 = 0.94$ **(Fig. B-1),** which was further applied to determine C using the actual mud weights. The drilling-mud resistivity and density are 0.282 Ω·m and 1.13 g/cm^3, respectively, taken at 24°C in the well used for the application example. The resistivity conversion to formation temperature was performed using the Arps (1953) formula for temperature (in °C), and the formation temperature was determined using Eq. B-2.

$$T_f = \Delta T \times D_f + T_s, \quad \text{(B-2)}$$

where T_f is the formation temperature, D_f is the formation depth (continuous), T_s is the mean local monthly surface temperature taken as –8.3°C for January (Fu et al. 2003), at the logging time for Well A, and the geothermal gradient ΔT is assumed to be 21.5°C/km (Feng et al. 2009).

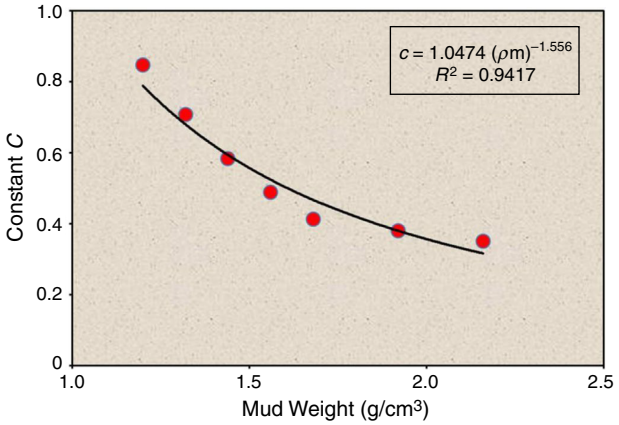

Fig. B-1—Determination of *C* in the correlation $R_{mf}=C(R_m)^{1.07}$ (Overton and Lipson 1958) using the data in Chart Gen-3 in Schlumberger (2009).

After we established the R_{mf}/depth profile, the R_w/depth profile was determined using a modified Bateman and Konen (1977) algorithm presented in Jorgensen (1988), and the related flow chart appearing therein in Fig. 5. This was conducted into several steps, as usual, including conversion of the R_{mf} into equivalent R_{mf} (R_{mfe}), calculation of R_w (R_{we}), and determination of R_w. With respect to the actual R_{mf} values, the following formulas were applied:

$$R_{mfe} = 0.85R_{mf}, \quad \text{(B-3)}$$

$$k = 0.24 \times T(\text{in } ^\circ\text{C}) + 65, \quad \text{(B-4)}$$

$$R_{we} = R_{mfe}10^{SP/k}, \quad \text{(B-5)}$$

$$R_w = \frac{75R_{we}+5}{146-337R_{we}}, \quad \text{if } R_{we} < 0.12, \quad \text{(B-6)}$$

$$R_w = -[(0.58-10)^{(0.69R_{we}-0.24)}] \quad \text{if } R_{we} > 0.12, \quad \text{(B-7)}$$

where SP is the spontaneous potential, and K is the electrochemical spontaneous-potential coefficient that depends on the formation temperature T_f (in °C). R_{mfe} and R_{we} are the calculated equivalent resistivities of the mud filtrate and formation water, respectively (both in Ω·m). The different resistivities were first calculated at 24°C, and then converted to the formation temperatures.